

2016

# Positive Feedforward Control Design For Stabilization Of A Single-Bus DC Power Distribution System Using An Improved Impedance Identification Technique

Silvia Arrúa

*University of South Carolina*

Follow this and additional works at: <http://scholarcommons.sc.edu/etd>



Part of the [Electrical and Computer Engineering Commons](#)

---

## Recommended Citation

Arrúa, S.(2016). *Positive Feedforward Control Design For Stabilization Of A Single-Bus DC Power Distribution System Using An Improved Impedance Identification Technique*. (Master's thesis). Retrieved from <http://scholarcommons.sc.edu/etd/3840>

This Open Access Thesis is brought to you for free and open access by Scholar Commons. It has been accepted for inclusion in Theses and Dissertations by an authorized administrator of Scholar Commons. For more information, please contact [SCHOLARC@mailbox.sc.edu](mailto:SCHOLARC@mailbox.sc.edu).

POSITIVE FEEDFORWARD CONTROL DESIGN FOR STABILIZATION OF A SINGLE-  
BUS DC POWER DISTRIBUTION SYSTEM USING AN IMPROVED IMPEDANCE  
IDENTIFICATION TECHNIQUE

by

Silvia Arrúa

Bachelor of Science  
National University of Asuncion, 2012

---

Submitted in Partial Fulfillment of the Requirements

For the Degree of Master of Science in

Electrical Engineering

College of Engineering and Computing

University of South Carolina

2016

Accepted by:

Enrico Santi, Director of Thesis

Andrea Benigni, Reader

Paul Allen Miller, Vice Provost and Interim Dean of Graduate Studies

© Copyright by Silvia Arrua, 2016  
All Rights Reserved.

## ACKNOWLEDGEMENTS

First, I would like to acknowledge my academic advisor Dr. Enrico Santi for his guidance and support during my first years as a graduate student and with whom I will continue working throughout my doctoral studies. I am pleased to be part of his group where I am continuously learning about different research areas.

Also, I would like to thank Dr. Andrea Benigni for his time and dedication as a part of my thesis committee.

## ABSTRACT

Due to recent advances in power electronics technology, DC power distribution systems offer distinct advantages over traditional AC systems for many applications such as electric vehicles, more electric aircrafts and industrial applications. For example, for the All-Electric ship proposed by the U.S. Navy the preferred design option is the adoption of a Medium Voltage DC power distribution system, due to the high power level required on board and the highly dynamic nature of the electric loads.

These DC power distribution systems consist of generation units, energy storage systems and different loads connected to one or more DC busses through switching power converters, providing numerous advantages in performance and efficiency. However, the growth of such systems comes with new challenges in the design and control areas. One problem is the potential instability caused by the interaction among feedback-controlled converters connected to the same DC bus.

Many criteria have been developed in the past to evaluate system stability. Additionally, passive or active solutions can be implemented to improve stability margins. One previously proposed solution is to implement Positive Feed-Forward (PFF) control in the load-side converter; with this technique it is possible to introduce a virtual damping impedance at the DC bus. A recently proposed design approach for PFF control is based on the Passivity Based Stability Criterion (PBSC), which analyzes passivity of the overall bus impedance to determine whether the system is stable or unstable.

However, since the PBSC does not provide direct information about system's dynamic performance, the PFF control design based on PBSC might lead to lightly damped systems. Therefore, a disturbance in the system may result in long-lasting lightly damped bus voltage oscillations. Moreover, in order to study the system dynamic performance it is necessary to know the bus impedance. A method has been proposed that uses digital network analyzer techniques and an additional converter that acts as a source for current injection to perturb the bus.

The present work provides original contributions in this area. First of all, the effect of the dominant poles of the bus impedance on the system dynamic performance is analyzed. A new closed-form design procedure is proposed for PFF control based on the desired location of these dominant poles that ensures a desired dynamic response with appropriate damping.

Regarding bus impedance identification using a switching converter for perturbation injection, a new technique is proposed that eliminates the need for an external converter to provide the excitation. The technique combines measurements performed by existing converters to reconstruct the overall bus impedance. Additionally, an improved perturbation technique utilizes multiple injections to eliminate the problems of injected disturbance rejection by the converter feedback loop at low frequency and the problem of attenuation due to reduced loop gain at high frequencies.

The proposed methods are validated using time domain simulations, in which the bus impedance of a single-bus DC power distribution system is estimated and then utilized for the design of a PFF controller to improve the dynamic characteristics.

## TABLE OF CONTENTS

ACKNOWLEDGEMENTS .....	iii
ABSTRACT .....	iv
LIST OF FIGURES .....	viii
LIST OF SYMBOLS .....	xi
LIST OF ABBREVIATIONS.....	xiii
CHAPTER 1: INTRODUCTION .....	1
1.1. DC power distribution systems .....	1
1.2. State of the art on stability analysis of DC power distribution systems.....	5
1.3. Positive Feed-Forward Control .....	8
1.4. Impedance Identification.....	10
1.5. Research Objectives .....	11
1.6. Contributions.....	12
CHAPTER 2: MODELLING AND STABILITY ANALYSIS .....	13
2.1. Unterminated small-signal modelling .....	13
2.2. Stability analysis .....	19
2.3. An illustrative example and simulation.....	22

CHAPTER 3: POSITIVE FEED-FORWARD CONTROL.....	29
3.1. Principle of PFF control .....	29
3.2. The design of the PFF control .....	32
3.3. An illustrative example and simulation.....	37
3.4. A decentralized implementation of PFF control .....	43
CHAPTER 4: SYSTEM IDENTIFICATION .....	46
4.1. Cross-correlation method .....	46
4.2. Maximum length Pseudo-Random Binary Sequences (PRBS) .....	48
4.3. Simplifications of the cross-correlation method .....	50
4.4. On-line impedance estimation using a double PRBS signal injection .....	52
4.5. An illustrative example and simulation.....	55
4.6. Design of PFF control .....	64
CHAPTER 5: CONCLUSIONS AND FUTURE WORK .....	67
5.1. Conclusions .....	67
5.2. Future Work .....	68
REFERENCES .....	69

## LIST OF FIGURES

Figure 1.1. Simplified MVCD system diagram. ....	3
Figure 1.2. Negative incremental input impedance due to CPL. ....	4
Figure 1.3. Interconnection of source and load subsystems. ....	5
Figure 1.4. (a) Single bus DC power distribution system, (b) equivalent source and load subsystems network, (c) equivalent 1-port network. ....	7
Figure 1.5. PRBS injection for bus impedance measurement .....	11
Figure 2.1. Small-signal model of an unterminated buck converter .....	14
Figure 2.2. Unterminated small-signal two-port model.....	15
Figure 2.3. Reduced block diagram for (a) open-loop operation, (b) inductor current feedback control, (c) output voltage feedback control.....	17
Figure 2.4. Small-signal model of a single bus DC system. ....	20
Figure 2.5. Equivalent source and load interacting subsystems representation using (a) circuital model and (b) block diagram.....	20
Figure 2.6. DC system with a source buck converter and two load buck converters. ....	22
Figure 2.7. Bus impedance Bode plot. ....	25
Figure 2.8. Poles and zeros of the bus impedance. ....	26
Figure 2.9. Nyquist plot of the minor loop gain $T_{MLG} = Z_S/Z_L$ . ....	27
Figure 2.10. Time domain simulation results in correspondence with a step in $V_{2ref}$ . ....	28
Figure 3.1. PFF control block diagram. ....	30
Figure 3.2. Unterminated small-signal model with PFF control. ....	32

Figure 3.3. Interacting subsystems representation with PFF control: (a) circuitual model, (b) reduced circuitual model and (c) block diagram. ....	33
Figure 3.4. Bus impedance Bode plot, with PFF control. ....	38
Figure 3.5. Poles and zeros of the bus impedance, with PFF control. ....	39
Figure 3.6. Improvement in the time domain simulation results with PFF control. ....	40
Figure 3.7. Bode plot of the input voltage-to-output voltage transfer function. ....	41
Figure 3.8. Feedback loop gain of $Buck_{LOAD1}$ . ....	42
Figure 3.9. Feedback loop gain of $Buck_{LOAD2}$ . ....	42
Figure 3.10. Poles and zeros of the bus impedance under FB control (blue) and FFFB (red). ....	43
Figure 3.11. Bus impedance under PFF control. ....	44
Figure 3.12. Time domain simulation results for scenarios (a), (b) and (c). ....	45
Figure 4.1. Linear time-invariant system. ....	47
Figure 4.2. PRBS signal. ....	49
Figure 4.3. Impedance measurement. ....	52
Figure 4.4. Single PRBS injection in the duty cycle signal for impedance estimation ....	53
Figure 4.5. Single PRBS injection in the FB reference signal for impedance estimation	54
Figure 4.6. Double injection of the PRBS signal for impedance estimation. ....	55
Figure 4.7. Bus current waveform. ....	56
Figure 4.8. Schematic representation of Test 1. ....	57
Figure 4.9. Schematic representation of Test 2. ....	58
Figure 4.10. Schematic representation of Test 3. ....	58
Figure 4.11. Test 1: Impedance identification results (dots) compared to the analytic expression (solid line) using (a) single PRBS injection and (b) double PRBS injection. ....	60

Figure 4.12. Test 2: Impedance identification results (dots) compared to the analytic expression (solid line) using (a) single PRBS injection and (b) double PRBS injection .....	60
Figure 4.13. Test 3: Impedance identification results (dots) compared to the analytic expression (solid line) using (a) single PRBS injection and (b) double PRBS injection .....	61
Figure 4.14. Estimated bus impedance (dots) compared to the analytic transfer function (solid).....	62
Figure 4.15. $Z_{bus}$ estimated (dots) and logarithmically thinned subset (x mark) .....	63
Figure 4.16. Parametric model of $Z_{bus}$ (dash) compared to the analytic model (solid). ..	64
Figure 4.17. Design of the damping impedance using the analytic model (blue) and the parametric model (red).....	65
Figure 4.18. Time domain simulation results with the implementation of PFF control obtained from the estimation of $Z_{bus}$ .....	66
Figure 5.1. Online tuning scheme. ....	68

## LIST OF SYMBOLS

$T_{MLG}$	Minor Loop Gain
$Z_{bus}$	Bus impedance
$Z_{damp}$	Damping impedance
$Z_{bus\_FF}$	Bus impedance with Positive Feedforward control
$\hat{v}_g$	Small-signal input voltage
$\hat{v}_{bus}$	Small-signal bus voltage
$\hat{v}$	Small-signal output voltage
$\hat{i}_{load}$	Small-signal load current
$\hat{d}$	Small-signal duty cycle
$\hat{i}_g$	Small-signal input current
$\hat{i}_L$	Small-signal inductor current
$\hat{i}_c$	Small-signal inductor current reference
$\hat{v}_{ref}$	Small-signal output voltage reference
$Z_{in}$	Input impedance transfer function
$G_{igi}$	Load current to input current transfer function
$G_{igd}$	Duty cycle to input current transfer function
$G_{igc}$	Control variable to input current transfer function under feedback control
$G_{vg}$	Input voltage to output voltage transfer function
$Z_{out}$	Output impedance transfer function

$G_{vd}$	Duty cycle to output voltage transfer function
$G_{vc}$	Control variable to output voltage transfer function under feedback control
$G_{iLg}$	Input voltage to inductor current transfer function
$G_{iLi}$	Load current to inductor current transfer function
$G_{iLd}$	Duty cycle to inductor current transfer function
$G_I$	Inductor current feedback controller transfer function
$G_V$	Output voltage feedback controller transfer function
$T_{FB}$	Feedback loop gain
$f_c$	Crossover frequency
$PM$	Phase margin
$\xi$	Damping factor
$Q$	Quality factor
$G_{CFF}$	Feedforward controller transfer function
$T_{FF}$	Feedforward gain
$D, D'$	Duty cycle and complementary duty cycle
$L, C, R$	Inductance, capacitance and resistance

## LIST OF ABBREVIATIONS

AC	.....	Alternating Current
AES	.....	All Electric Ship
CM	.....	Current Mode Feedback Control
CPL	.....	Constant Power Load
DC	.....	Direct Current
DFT	.....	Discrete Fourier Transform
ESAC	.....	Energy Source Analysis Consortium
FB	.....	Feedback Control
FFT	.....	Fast Fourier Transform
MVDC	.....	Medium Voltage Direct Current
OL	.....	Open loop
PBSC	.....	Passivity Based Stability Criterion
PFF	.....	Positive Feedforward
PRBS	.....	Pseudo Random Binary Sequence
RHP	.....	Right Half Plane
ZID	.....	Impedance Identification

# CHAPTER 1

## INTRODUCTION

This introductory chapter discusses the issues related to stability in DC Power Distribution Systems and its effects on the normal operation of such systems. The following sections provide a literature review of stability analysis and methods that were proposed to improve stability margins, as well as a review of impedance identification techniques which will be used for the design of a stabilizer controller. Finally, the objectives and contributions of this work are stated.

### 1.1. DC Power Distribution Systems

The development of power semiconductor devices provided several advantages for DC power distribution systems over traditional AC systems [1], especially in applications where high efficiency and reduced size and weight are critical, for example in the avionic field where the concept of the more electric aircraft has been developed.

Another application where the use of DC distribution systems is a main focus of research is the All-Electric Ship (AES) proposed by the U.S. Navy, where power electronics has a big impact on system performance, enabling the possibility to effectively control the power flow in the system [2].

In conventional mechanically propelled ships the electrical power system played a limited role. DC power distribution was used for low power applications and AC power distribution for higher power levels.

The introduction of power electronic converters for marine applications has led to a revolution in the onboard power system design starting from the use of electric propulsion, providing several advantages such as better dynamic response and lower vibrations, among others.

Furthermore, the concept of the All-Electric Ship, offers unprecedented advantages from the point of view of efficiency and flexibility of operation.

With the introduction of power electronics, the DC power distribution system has become a competitive alternative, allowing a simplified connection and disconnection of different types and sizes of generators and storage devices, elimination of large transformers and voltage droop due to reactive power, reduction of fuel consumption and elimination of phase angle synchronization requirement in case of multiple generators. The capability of power electronics to control and interrupt current also lead to a reduction of size and ratings of switchgears.

The adoption of voltage higher than 1kV is necessary due to the high power levels required in modern All-Electric Ships, leading to the Medium Voltage DC (MVDC) distribution shown in **Figure 1.1**. This type of onboard distribution system integrates several groups of power sources, energy storage systems and loads, all connected to the main DC bus through power electronic converters.

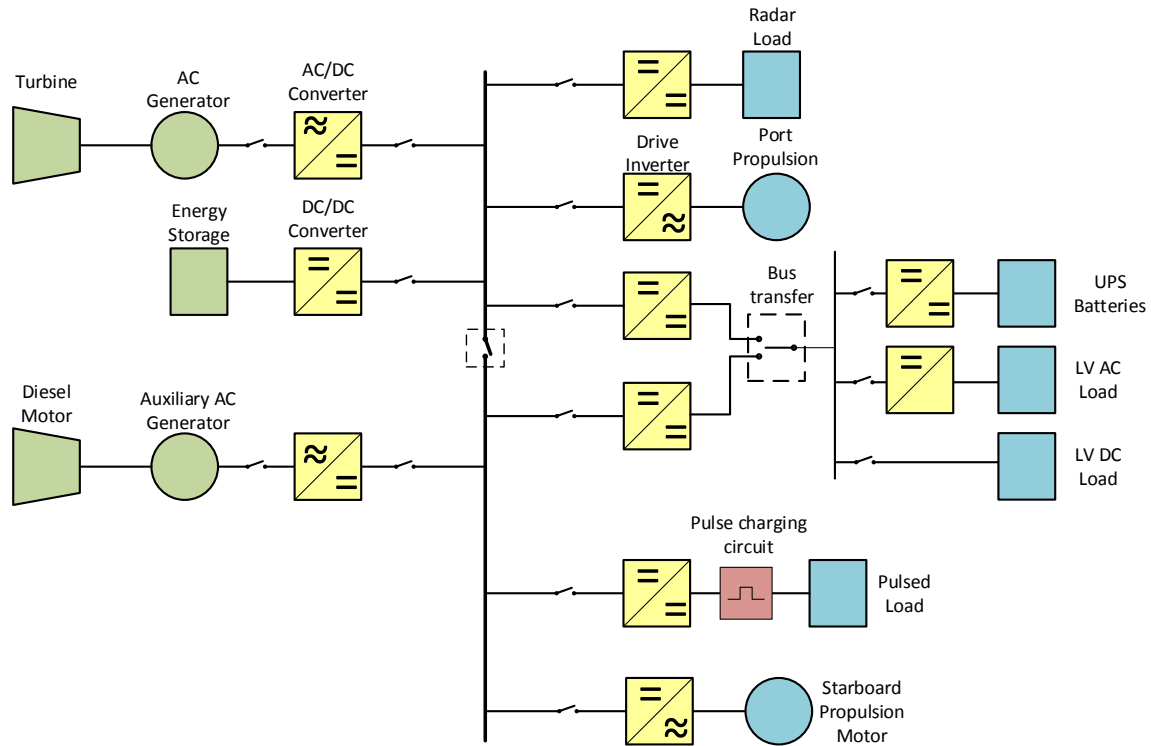


**Figure 1.1. Simplified MVCD system diagram.**

The use of DC systems is not limited to the specific applications mentioned; actually, there has been an increase exploitation of the capabilities of DC power systems, integrating them with the already existent AC grid, resulting in a safer, more reliable, flexible and controllable power grid.

With the development of renewable generation and energy storage, DC interconnection grids are being installed for residential and industrial purposes, due to its advantages, incorporating three kinds of power distribution systems: full AC, full DC and hybrid AC-DC systems [3].

The growth of DC systems creates new challenges. In particular the subsequent increase number of interconnected power electronic devices, as shown in **Figure 1.1**, affects systems dynamics. Although each converter is designed to be standalone stable, the interaction among converters becomes an issue and is the cause of potential system instability because of the Constant Power Load (CPL) effect [4], related to the interaction among the feedback loops of the various switching converters.

Switching power converters with a tight output voltage regulation behave as constant power loads ( $P = VI = \text{constant}$ ) at the input terminals, so the input impedance has a negative incremental resistance characteristic ( $dV/dI < 0$ ), even though its instantaneous impedance is always positive ( $V/I > 0$ ), as shown in **Figure 1.2** [5]. When interacting with a source impedance at the input ports of the switching converter, under certain conditions the net bus impedance can become a negative resistor and oscillation will occur [4].

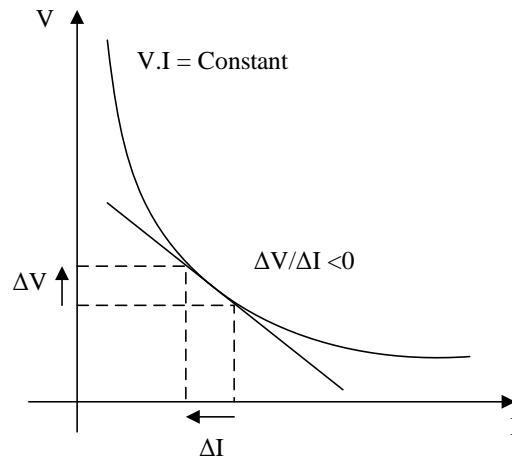


**Figure 1.2. Negative incremental input impedance due to CPL.**

1.2. State of the art on stability analysis of DC power distribution systems

In the stability analysis, DC systems can be considered as consisting of a source subsystem and load subsystem connected to a main DC bus, as shown in **Figure 1.3**.

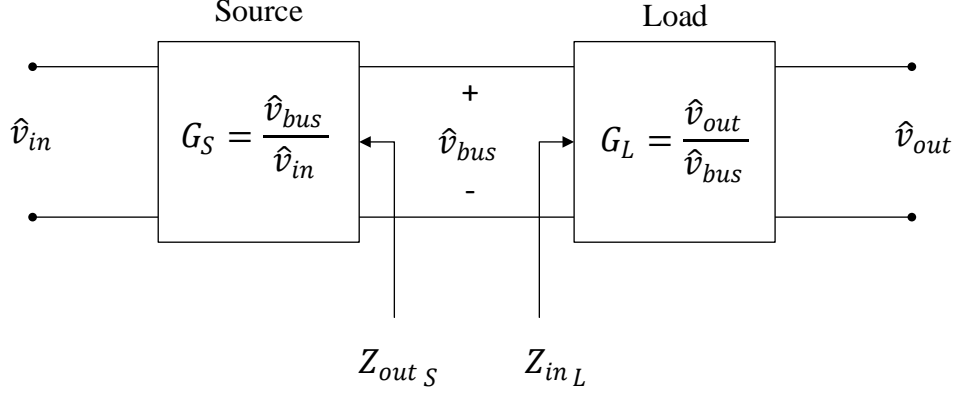


**Figure 1.3. Interconnection of source and load subsystems.**

Consider the simple case of a system composed by two converters, the source converter establishes the bus voltage and the load converter feeds a load at a different voltage level.

Each converter has its own input-to-output transfer function determined from the small-signal characteristics. The input-to-output transfer function of the cascaded system is:

$$G = \frac{\hat{v}_{out}}{\hat{v}_{in}} = G_S G_L \frac{Z_{in_L}}{Z_{in_L} + Z_{out_S}} = G_S G_L \frac{1}{1 + T_{MLG}} \quad (1.1)$$

Where  $T_{MLG} = Z_{out_S}/Z_{in_L}$  is called the Minor Loop Gain.

If the converters are designed to be standalone stable, the stability of the cascaded system depends on  $T_{MLG}$ . The Nyquist criterion provides a necessary and sufficient

condition for stability: the system in (1.1) is stable if and only if the Nyquist contour of  $T_{MLG}$  does not encircle the  $(-1,0)$  point [6].

In [4], the addition of line input filters to feedback-controlled switching converters with negative input resistance at low frequencies is analyzed. Design inequalities are proposed to ensure system stability and that the converter properties are essentially unaffected by the addition of the input filter. In particular (1.2) is proposed as a sufficient condition (small loop gain) to satisfy the Nyquist criterion for stability.

$$\|T_{MLG}\| = \left\| \frac{Z_{outS}}{Z_{inL}} \right\| \ll 1 \quad (1.2)$$

Although (1.2) ensures stability, it may result in a conservative design. A lot of work has been done to establish sufficient conditions for stability defining forbidden regions for the Nyquist contour of  $T_{MLG}$  in the  $s$ -plane, like the Gain Margin and Phase Margin criterion, the Opposing Argument Criterion, the Energy Source Analysis Consortium (ESAC) Criterion, and the Three Step Impedance Criterion. A review of these criteria is provided in [6].

All minor-loop-gain based stability criteria impose stability conditions on the load-impedance/source-impedance ratio and define specifications for the load impedance for a given source impedance, or vice-versa. They implicitly assume a given power flow direction, which may be considered as a disadvantage in cases where the role of source and load vary during converter operation, like for example in energy storage subsystems.

The recently proposed Passivity Based Stability Criterion (PBSC) [7] analyzes passivity of the bus impedance on a single-bus DC power distribution like in **Figure 1.4(a)**; the given system can be reduced to an equivalent source subsystem and load

subsystem network (**Figure 1.4(b)**), and then to an equivalent 1-port network (**Figure 1.4(c)**).

The resulting bus impedance is the parallel combination of all converters impedances seen from the DC bus.

$$Z_{bus} = Z_{S1} // Z_{S2} // \dots // Z_{Sn} // Z_{L1} // \dots // Z_{Lm} \quad (1.3)$$

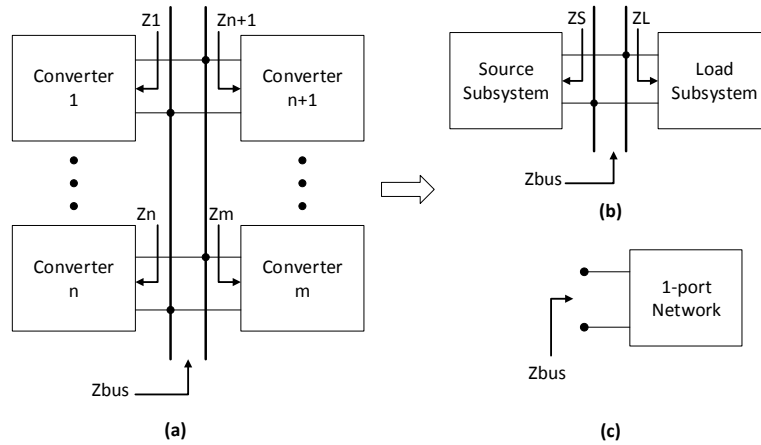


**Figure 1.4. (a) Single bus DC power distribution system, (b) equivalent source and load subsystems network, (c) equivalent 1-port network.**

For the time invariant 1-port network of **Figure 1.4(c)** to be passive the following conditions must be satisfied:

- a)  $Z_{bus}(s)$  has no right half plane (RHP) poles, and
- b)  $Z_{bus}(s)$  has a Nyquist contour which wholly lies in the closed RHP, implying that the phase of  $Z_{bus}(s)$  must be between  $-90^\circ$  and  $90^\circ$  at all frequencies

A passive network is also stable; therefore, the PBSC is a sufficient condition for stability of the overall system. Notice that this is a sufficient but not necessary condition; a stable system is not necessarily passive at all frequencies.

In [8] a practical PBSC is proposed, based on the passivity condition of  $Z_{bus}(s)$  in a limited range of frequencies around the resonant frequency of the system.

The main advantages of the PBSC over the minor loop gain based stability criteria are that it can easily handle multiple interconnected converters and inversion of power flow direction, the bus impedance online measurement is easy to implement, and it can lead to the design of virtual damping impedances to improve system stability. However, it does not provide direct information about the dynamic performance of the system.

### 1.3. Positive Feed-Forward Control

Passive and active methods are proposed in the literature for stability improvement. Passive approaches consist in the use of resistive, capacitive and inductive components in the DC link between the source and load subsystems, which can be relatively easy to implement but may cause significant power dissipation.

Active approaches can be divided in two categories: a power buffer can be added between source and load subsystems, decoupling them; or a modification of the control scheme of the source and/or load converter can be implemented. On the one hand, the second approach is usually more economical, since it does not require an additional power stage. On the other hand, the implementation of active methods can be very complex and sometimes cause a conflict with other control objectives.

Use of Positive Feed-Forward (PFF) control as an active approach for stability improvement is presented in [8] [9] [10] [11]. The PFF control actively introduces a virtual damping impedance  $Z_{damp}$  at the input ports of the switching power converter where it is implemented, as shown later in Chapter 3. By proper design of this damping impedance, the system can be stabilized [8].

### 1.3.1. PFF control design based on the PBSC

A method for designing PFF control is proposed in [8] based on the desired passivity condition of the bus impedance of a single-bus power distribution system. The objective of the controller is to modify the overall bus impedance only in a frequency range around the resonant frequency like in (1.4), by introducing a virtual damping impedance  $Z_{damp}$  using PFF control.

$$\frac{1}{Z_{bus\_FF}} = \frac{1}{Z_{bus}} + \frac{1}{Z_{damp}}$$

$$\frac{1}{Z_{bus\_FF}} = \begin{cases} \frac{1}{Z_{bus}} & \text{at low frequencies} \\ \frac{1}{Z_{damp}} & \text{at } \omega = \omega_{res} \\ \frac{1}{Z_{bus}} & \text{at high frequencies} \end{cases}$$
(1.4)

$Z_{damp}$  is designed to dominate at the resonant frequency  $\omega_{res}$  so that the passivity condition is met  $-90^\circ < \arg[Z_{bus\_FF}(j\omega_{res})] < 90^\circ$ , while leaving the bus impedance unchanged at low and high frequencies.

The procedure starts from the choice of a desired crossover frequency for the load subsystem, which means desired output performance, in presence of source impedance and PFF control.

In order to obtain good passivation effect, the chosen crossover frequency has to be smaller than the resonant frequency of the system. If a good tradeoff between stability improvement, determined by the passivity condition, and output performance is obtained, the procedure is complete, otherwise it has to be iterated starting from the choice of a

different crossover frequency. This method was proven to provide a stabilizing effect on DC systems, however, if the objective of the controller is to provide the system with a certain damping level for bus oscillations, the process becomes iterative and different crossover frequencies have to be chosen until a good dynamic performance is reached.

#### 1.4. Impedance Identification

Power systems parameters vary over time due to load changes, system reconfiguration, component aging, failure, and so on. These variations affect the impedances of the source and load subsystems as seen from the DC bus.

System identification is a very powerful technique that allows on-line estimation of systems' parameters; obtaining input/output impedances of power converters connected to a specific DC bus and the overall bus impedance are particularly important for stability analysis purpose.

An extension to the cross-correlation method of switching converter identification, allowing online monitoring of Thévenin source equivalents and load impedances is presented in [12] [13]. The method implements a Pseudo Random Binary Sequence (PRBS) test signal as a white noise approximation and the impedances are obtained by measuring voltages and currents variations. In [14] an additional converter is used as a current source to perturb the bus in order to measure the overall bus impedance of the equivalent 1-port network as in **Figure 1.5**.

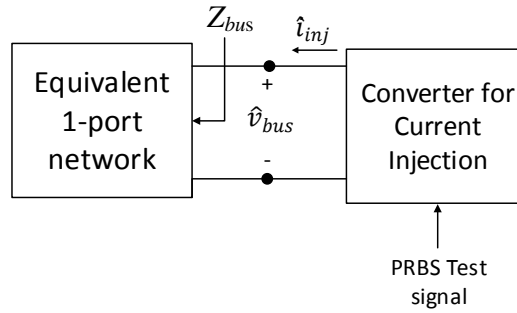


**Figure 1.5. PRBS injection for bus impedance measurement**

The parametric model is obtained from the non-parametric frequency response data by using the method of Least Squares Fitting. A logarithmic thinning process is proposed in [14] to enforce equal fitting priority across the frequency range of interest and to reduce the computational requirements of the numerical fitting algorithm.

When using feedback-controlled converters for system identification, the point of injection of the PRBS signal is of significant importance for the accuracy of the measurements, since the feedback loop causes a rejection of disturbances at low frequencies.

### 1.5. Research Objectives

The general objectives of this work are:

- To improve the dynamic performance of DC power distribution systems by implementing a stabilizer controller that will ensure specific dynamic characteristics,
- To increase the accuracy of online, non-parametric impedance identification for a wide range of frequencies, and

- To eliminate the need of additional converters in the estimation of the bus impedance of DC power distribution systems.

#### 1.6. Contributions

The main contributions consist of:

- A design method for Positive Feed-Forward control using a closed-form procedure, based on the desired damping for bus oscillations,
- An improved perturbation technique using multiple injections to increase the identification accuracy, and
- Bus impedance identification combining measurements from existing converters.

## CHAPTER 2

### MODELLING AND STABILITY ANALYSIS

This chapter describes the general procedure to obtain a small-signal model of a DC power distribution system. The procedure is then applied to a DC power system to investigate its dynamic performance based on the analysis of the bus impedance transfer function and time domain simulations.

#### 2.1. Unterminated small-signal modelling

A methodology that provides flexibility for modelling a large DC power distribution system is proposed in [15], based on the small-signal representation of unterminated power converters. This technique will be used to obtain an analytic model of a single-bus DC power distribution system, allowing the analysis of the effect of the bus impedance transfer function in the dynamic characteristic of such system.

An unterminated buck converter, part of a larger system, and its corresponding averaged small-signal ac model for continuous conduction mode are shown in **Figure 2.1** as an example. The small-signal model is obtained by perturbation and linearization around the steady state operating point [16].

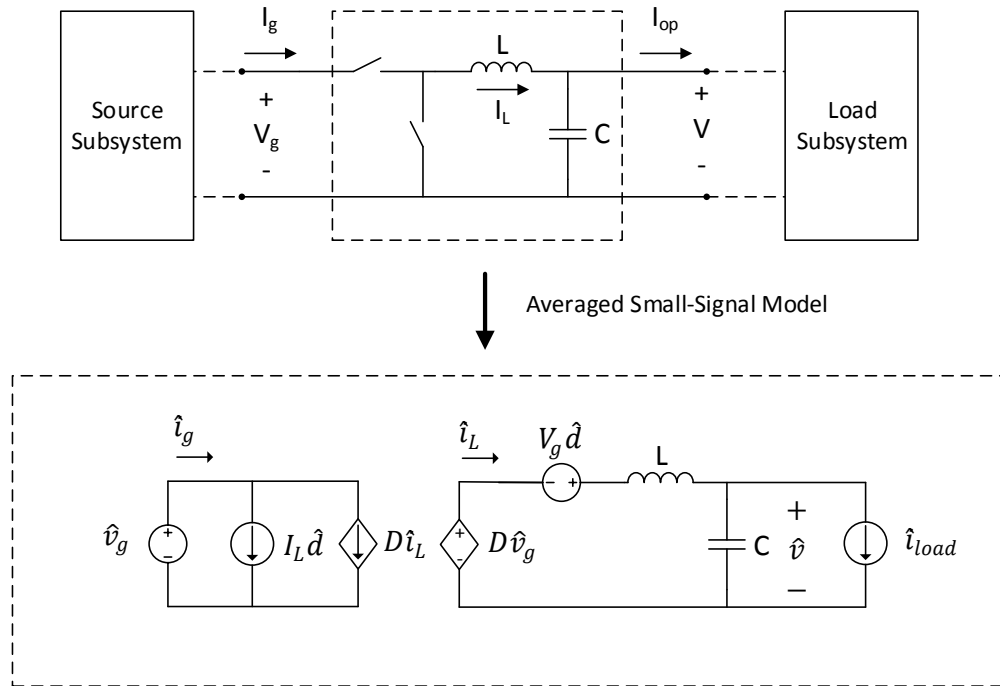


**Figure 2.1. Small-signal model of an unterminated buck converter**

The small-signal model of Figure 2.1 is equivalently represented as a two-port network like in Figure 2.2, where the input variables are perturbations on input voltage  $\hat{v}_g$ , on load current  $\hat{i}_{load}$  and on duty cycle  $\hat{d}$ , and the output variables are the output voltage  $\hat{v}$  and the input current  $\hat{i}_g$ .

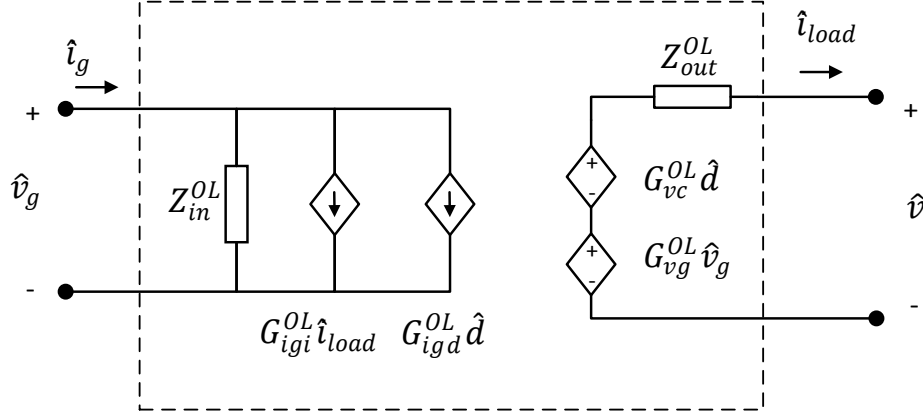


**Figure 2.2. Underterminated small-signal two-port model**

The expression (2.1) relates the input and output variables of the small-signal model. OL stands for open loop operation of the converter. For control purposes is desirable to obtain the inductor current  $\hat{i}_L$  as an output variable.

$$\begin{bmatrix} \hat{i}_g \\ \hat{v} \\ \hat{i}_L \end{bmatrix} = \begin{bmatrix} 1/Z_{in}^{OL} & G_{igi}^{OL} & G_{igd}^{OL} \\ G_{vg}^{OL} & -Z_{out}^{OL} & G_{vd}^{OL} \\ G_{iLg}^{OL} & G_{iLi}^{OL} & G_{iLd}^{OL} \end{bmatrix} \cdot \begin{bmatrix} \hat{v}_g \\ \hat{i}_{load} \\ \hat{d} \end{bmatrix}$$

(2.1)

The following table presents the transfer functions in (2.1) and Figure 2.2 for the cases of a buck, boost and buck-boost converter. In these expressions, the steady-state capacitor voltage  $V$ , inductor current  $I_L$ , duty cycle  $D$  and the complement of the duty cycle  $D'=1-D$  are considered.

**Table 2.1. Open-loop unterminated transfer functions.**

	<i>Buck</i>	<i>Boost</i>	<i>Buck-Boost</i>
$1/Z_{in}^{OL}(s)$	$D^2 \frac{Cs}{LCs^2 + 1}$	$\frac{1}{D'^2} \frac{sC}{LCs^2 + 1}$	$\frac{D^2}{D'^2} \frac{sC}{LCs^2 + 1}$
$G_{igi}^{OL}(s)$	$\frac{D}{LCs^2 + 1}$	$\frac{1}{D'} \frac{1}{LCs^2 + 1}$	$-\frac{D}{D'} \frac{1}{LCs^2 + 1}$
$G_{igd}^{OL}(s)$	$I_L + V \frac{Cs}{LCs^2 + 1}$	$\frac{1}{D'^2} \frac{VCs + D'I_L}{LCs^2 + 1}$	$I_L + \frac{1}{D'^2} \frac{D'DI_L - VCs}{LCs^2 + 1}$
$G_{vg}^{OL}(s)$	$\frac{D}{LCs^2 + 1}$	$\frac{1}{D'} \frac{1}{LCs^2 + 1}$	$-\frac{D}{D'} \frac{1}{1 + s^2 \frac{LC}{D'^2}}$
$Z_{out}^{OL}(s)$	$\frac{Ls}{LCs^2 + 1}$	$\frac{1}{D'^2} \frac{sL}{LCs^2 + 1}$	$\frac{1}{D'^2} \frac{sL}{1 + s^2 \frac{LC}{D'^2}}$
$G_{vd}^{OL}(s)$	$\frac{V}{D} \frac{1}{LCs^2 + 1}$	$\frac{1}{D'^2} \frac{D'V - LI_L s}{LCs^2 + 1}$	$\frac{V}{D'D} \frac{1}{1 + s^2 \frac{LC}{D'^2}}$
$G_{iLg}^{OL}(s)$	$D \frac{Cs}{LCs^2 + 1}$	$\frac{1}{D'^2} \frac{sC}{LCs^2 + 1}$	$\frac{D}{D'^2} \frac{sC}{LCs^2 + 1}$
$G_{iLi}^{OL}(s)$	$\frac{1}{LCs^2 + 1}$	$\frac{1}{D'} \frac{1}{LCs^2 + 1}$	$-\frac{1}{D'} \frac{1}{LCs^2 + 1}$
$G_{iLd}^{OL}(s)$	$\frac{V}{D} \frac{Cs}{LCs^2 + 1}$	$\frac{1}{D'^2} \frac{VCs + D'I_L}{LCs^2 + 1}$	$\frac{1}{DD'^2} \frac{D'DI_L - VCs}{LCs^2 + 1}$

A multi-loop negative feedback control is considered in this work in order to achieve a desired output behavior; an inner loop is designed to regulate the inductor

current and an outer loop is designed to regulate the output voltage; the control scheme is shown in **Figure 2.3**. The design of the feedback control is done to obtain a certain phase and gain margins and for a specific power level (operating point) of the standalone converter.

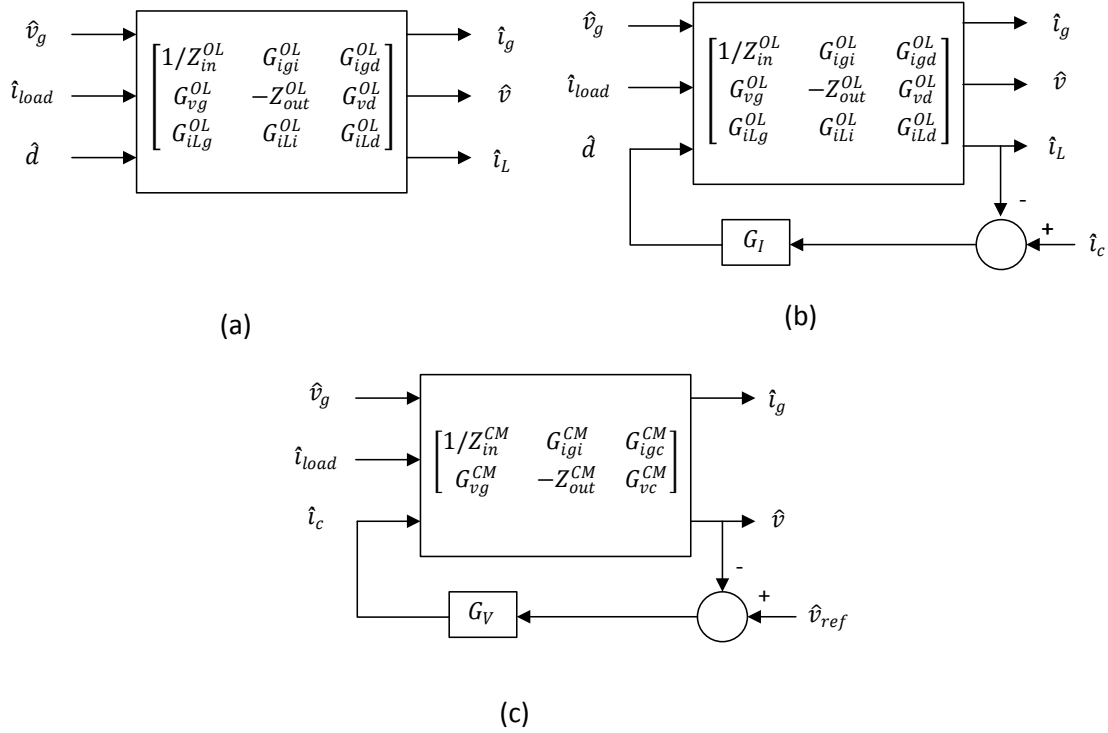


**Figure 2.3. Reduced block diagram for (a) open-loop operation, (b) inductor current feedback control, (c) output voltage feedback control.**

With the inductor current feedback, the relation between inputs and outputs is (2.2), notice that the inductor current is not included as an output anymore.

$$\begin{bmatrix} \hat{i}_g \\ \hat{v} \end{bmatrix} = \begin{bmatrix} 1/Z_{in}^{CM} & G_{igi}^{CM} & G_{igc}^{CM} \\ G_{vvg}^{CM} & -Z_{out}^{CM} & G_{vc}^{CM} \end{bmatrix} \cdot \begin{bmatrix} \hat{v}_g \\ \hat{i}_{load} \\ \hat{i}_c \end{bmatrix} \quad (2.2)$$

The transfer functions in (2.2) are given by:

$$\frac{1}{Z_{in}^{CM}} = \frac{1}{Z_{in}^{OL}} - \frac{G_{igd}^{OL} G_{iLg}^{OL}}{G_{iLd}^{OL}} \frac{T_{PI}}{T_{PI} + 1} \quad (2.3)$$

$$G_{igi}^{CM} = G_{igi}^{OL} - \frac{G_{igd}^{OL} G_{iLi}^{OL}}{G_{iLd}^{OL}} \frac{T_{PI}}{T_{PI} + 1} \quad (2.4)$$

$$G_{igc}^{CM} = \frac{G_{igd}^{OL}}{G_{iLd}^{OL}} \frac{T_{PI}}{T_{PI} + 1} \quad (2.5)$$

$$G_{vg}^{CM} = G_{vg}^{OL} - \frac{G_{vd}^{OL} G_{iLg}^{OL}}{G_{iLd}^{OL}} \frac{T_{PI}}{T_{PI} + 1} \quad (2.6)$$

$$Z_{out}^{CM} = Z_{out}^{OL} + \frac{G_{vd}^{OL} G_{iLi}^{OL}}{G_{iLd}^{OL}} \frac{T_{PI}}{T_{PI} + 1} \quad (2.7)$$

$$G_{vc}^{CM} = \frac{G_{vd}^{OL}}{G_{iLd}^{OL}} \frac{T_{PI}}{T_{PI} + 1} \quad (2.8)$$

Where  $T_{PI}$  is the current mode feedback loop gain given by:

$$T_{PI} = G_I G_{iLd}^{OL} \quad (2.9)$$

As a last step the output voltage feedback is included, so the model becomes (2.10), and the closed loop transfer functions are given by (2.11) to (2.16).

$$\begin{bmatrix} \hat{i}_g \\ \hat{v} \end{bmatrix} = \begin{bmatrix} \frac{1}{Z_{in}^{FB}} & G_{igi}^{FB} & G_{igc}^{FB} \\ G_{vg}^{FB} & -Z_{out}^{FB} & G_{vc}^{FB} \end{bmatrix} \cdot \begin{bmatrix} \hat{v}_g \\ \hat{i}_{load} \\ \hat{v}_{ref} \end{bmatrix} \quad (2.10)$$

$$\frac{1}{Z_{in}^{FB}} = \frac{1}{Z_{in}^{CM}} - \frac{G_{igc}^{CM} G_{vg}^{CM}}{G_{vc}^{CM}} \frac{T_{FB}}{T_{FB} + 1} \quad (2.11)$$

$$G_{igi}^{FB} = G_{igi}^{CM} + \frac{G_{igc}^{CM} Z_{out}^{CM}}{G_{vc}^{CM}} \frac{T_{FB}}{T_{FB} + 1} \quad (2.12)$$

$$G_{igc}^{FB} = \frac{G_{igc}^{CM}}{G_{vc}^{CM}} \frac{T_{FB}}{T_{FB} + 1} \quad (2.13)$$

$$G_{vg}^{FB} = \frac{G_{vg}^{CM}}{T_{FB} + 1} \quad (2.14)$$

$$Z_{out}^{FB} = \frac{Z_{out}^{CM}}{T_{FB} + 1} \quad (2.15)$$

$$G_{vc}^{FB} = \frac{T_{FB}}{T_{FB} + 1} \quad (2.16)$$

In these expressions  $T_{FB}$  is the voltage feedback loop gain given by (2.17), which will determine the output performance of the converter

$$T_{FB} = G_V G_{vc}^{CM} \quad (2.17)$$

## 2.2. Stability analysis

The representation of a large DC power distribution system can be built using the unterminated model [14]. Considering a single-bus DC system consisting of a source converter that controls the bus voltage and a load subsystem made of two converters terminated with generic impedances, the representation is shown in **Figure 2.4** where  $\hat{c}$  is a generic control variable, therefore the model can be considered open loop or feedback controlled.

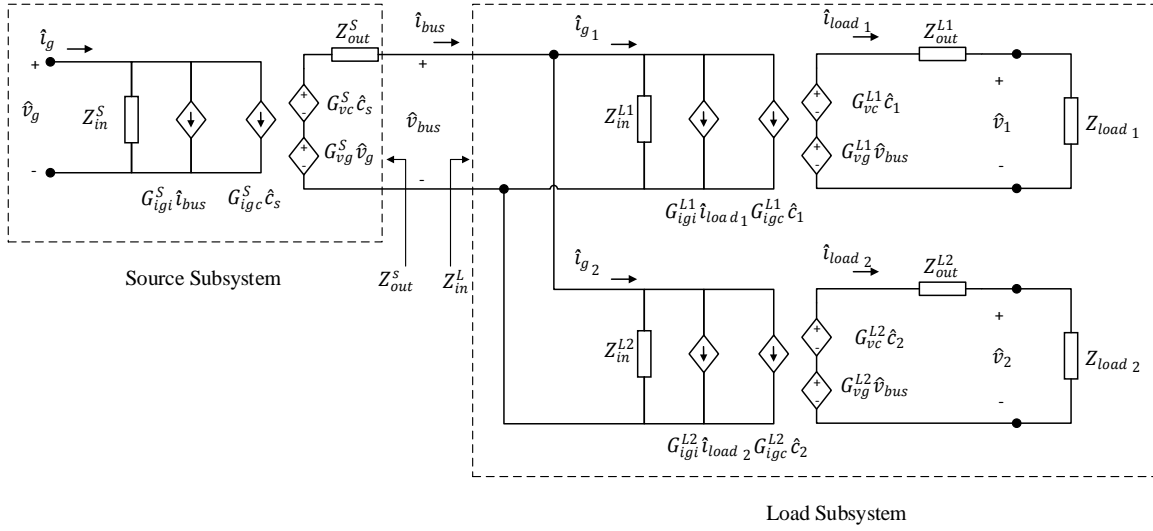


**Figure 2.4. Small-signal model of a single bus DC system.**

**Figure 2.5(a)** is a simplified representation of the cascaded system that is also equivalent to the block diagram in **Figure 2.5(b)**. In these figures the source and load subsystems are represented using the Thévenin equivalent and the Norton equivalent respectively.

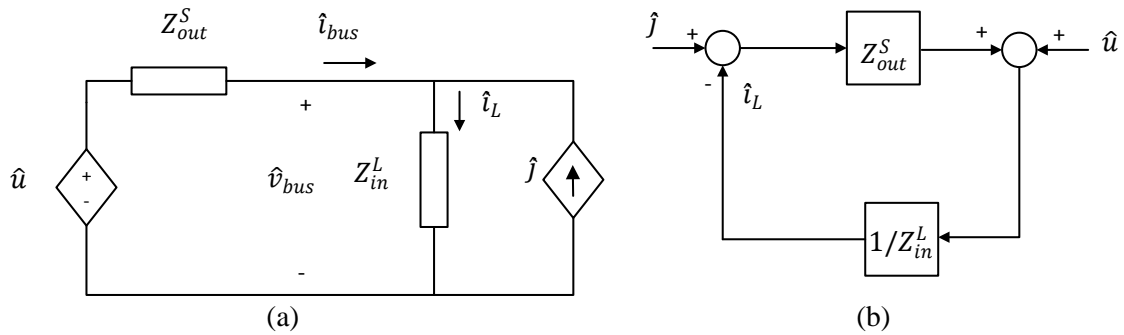


**Figure 2.5. Equivalent source and load interacting subsystems representation using (a) circuitual model and (b) block diagram**

A review of the classical study on the stability of interacting subsystems is provided in [8] using the representation from **Figure 2.5**.

For the analysis, it is assumed that the load subsystem is designed to be standalone stable, meaning that the load current is stable when powered from an ideal source.

The feedback system in **Figure 2.5(b)** is internally stable if and only if the transfer function matrix (2.18) is exponentially stable [16]:

$$\begin{bmatrix} \hat{i}_L \\ \hat{v}_{bus} \end{bmatrix} = \begin{bmatrix} \frac{Z_{out}^S}{Z_{in}^L} \frac{1}{1 + \frac{Z_{out}^S}{Z_{in}^L}} & \frac{1}{Z_{in}^L} \frac{1}{1 + \frac{Z_{out}^S}{Z_{in}^L}} \\ \frac{Z_{out}^S}{1 + \frac{Z_{out}^S}{Z_{in}^L}} & \frac{1}{1 + \frac{Z_{out}^S}{Z_{in}^L}} \end{bmatrix} \cdot \begin{bmatrix} \hat{j} \\ \hat{u} \end{bmatrix} \quad (2.18)$$

According to this definition each of the four transfer functions in (2.18) must be exponentially stable. If  $Z_{out}^S$  and  $1/Z_{in}^L$  are both unstable, then it is necessary to check all four of these transfer functions. However, if at least one of them is stable this condition can be alleviated. Since  $1/Z_{in}^L$  is assumed to be stable, the feedback system in **Figure 2.5(b)** is internally stable if and only if the third term of the matrix (2.18) is exponentially stable. This term resembles the bus impedance transfer function given by (2.19).

$$Z_{bus} = \frac{Z_{out}^S}{1 + \frac{Z_{out}^S}{Z_{in}^L}} \quad (2.19)$$

In conclusion, exponential stability of  $Z_{bus}(s)$  implies internal stability of the interacting system in **Figure 2.4** providing that the load subsystem is standalone stable.

Also comparing (2.19) with (1.1), the dominant poles of the bus impedance will determine the dynamics of the cascaded system.

### 2.3. An illustrative example and simulation

As an illustrative example, the dc system shown in **Figure 2.6** is considered; a source buck converter “ $Buck_{SOURCE}$ ” with input voltage  $V_{in} = 200$  V, regulates the voltage of a main DC bus to  $V_{bus} = 100$  V. Two buck converters, “ $Buck_{LOAD1}$ ” and “ $Buck_{LOAD2}$ ”, are connected to the DC bus and feed resistive loads at different voltage levels. The figure shows the values of the power stage components and the switching frequency is 20 kHz. A multi-loop control scheme is implemented, consisting in an inner current loop and an outer voltage loop PI control strategy. The current and voltage feedbacks are designed according to the specifications given in **Table 2.** The regulated output voltages are 54.77V for “ $Buck_{LOAD1}$ ” and 41.23V for “ $Buck_{LOAD2}$ ”.

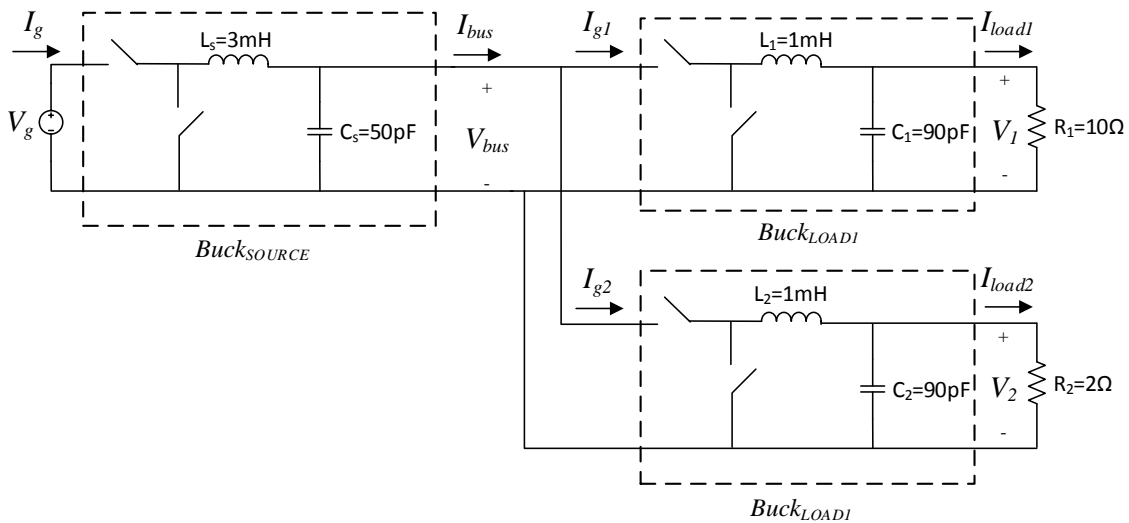


**Figure 2.6.** DC system with a source buck converter and two load buck converters.

**Table 2.2. Feedback control design specifications.**

	Current Feedback	Voltage Feedback
$Buck_{source}$	$f_{c_I} = 1kHz$ $PM_I = 80^\circ$	$f_{c_V} = 0.25kHz$ $PM_V = 80^\circ$
$Buck_{Load_1}$	$f_{c_I} = 1kHz$ $PM_I = 80^\circ$	$f_{c_V} = 0.1kHz$ $PM_V = 80^\circ$
$Buck_{Load_2}$	$f_{c_I} = 1kHz$ $PM_I = 80^\circ$	$f_{c_V} = 0.1kHz$ $PM_V = 80^\circ$

The small-signal model of the cascaded system given in **Figure 2.4** is described by the equations in (2.20).

$$\left\{ \begin{array}{l} \hat{i}_g = \frac{1}{Z_{in_s}^{FB}} \hat{v}_g + G_{igi_s}^{FB} \hat{i}_{bus} + G_{igc_s}^{FB} \hat{v}_{ref} \\ \hat{v}_{bus} = G_{vg_s}^{FB} \hat{v}_g - Z_{out_s}^{FB} \hat{i}_{bus} + G_{vc_s}^{FB} \hat{v}_{ref} \\ \hat{i}_{bus} = \hat{i}_{g_1} + \hat{i}_{g_2} \end{array} \right.$$

$$\left\{ \begin{array}{l} \hat{i}_{g_1} = \frac{1}{Z_{in_1}^{FB}} \hat{v}_{bus} + G_{igi_1}^{FB} \hat{i}_{load_1} + G_{igc_1}^{FB} \hat{v}_{1ref} \\ \hat{v}_1 = G_{vg_1}^{FB} \hat{v}_{bus} - Z_{out_1}^{FB} \hat{i}_{load_1} + G_{vc_1}^{FB} \hat{v}_{1ref} \\ \hat{i}_{load_1} = \frac{\hat{v}_1}{R_1} \end{array} \right.$$

$$\begin{cases} \hat{i}_{g_2} = \frac{1}{Z_{in_2}^{FB}} \hat{v}_{bus} + G_{igi_2}^{FB} \hat{i}_{load_2} + G_{igc_2}^{FB} \hat{v}_{2ref} \\ \hat{v}_2 = G_{vg_2}^{FB} \hat{v}_{bus} - Z_{out_2}^{FB} \hat{i}_{load_2} + G_{vc_2}^{FB} \hat{v}_{2ref} \\ \hat{i}_{load_2} = \frac{\hat{v}_2}{R_2} \end{cases} \quad (2.20)$$

The load input impedances seen from the DC bus are given by (2.21) and (2.22) due to the resistors  $R_1$  and  $R_2$ .

$$\frac{1}{Z_{in_T}^{L1}} = \frac{1}{Z_{in_1}^{FB}} + \frac{G_{igi_1}^{FB} G_{vg_1}^{FB}}{R_1 + Z_{out_1}^{FB}} \quad (2.21)$$

$$\frac{1}{Z_{in_T}^{L2}} = \frac{1}{Z_{in_2}^{FB}} + \frac{G_{igi_2}^{FB} G_{vg_2}^{FB}}{R_2 + Z_{out_2}^{FB}} \quad (2.22)$$

The degradation of the stability margin of the system caused by the interaction between source and the load subsystems will be analyzed by determining the bus impedance. A step in the reference voltage of  $Buck_{LOAD2}$  is applied in a time domain simulation to examine the dynamic performance.

In **Figure 2.7**, the source output impedance is compared to the input impedance of the load subsystem which corresponds to  $Z_{in_T}^{L1}$  in parallel with  $Z_{in_T}^{L2}$ . The solid line corresponds to the bus impedance, built by the parallel combination of the source output impedance and the load subsystem input impedance as:

$$\frac{1}{Z_{bus}} = \frac{1}{Z_{out}^S} + \frac{1}{Z_{in_T}^{L1}} + \frac{1}{Z_{in_T}^{L2}} \quad (2.23)$$

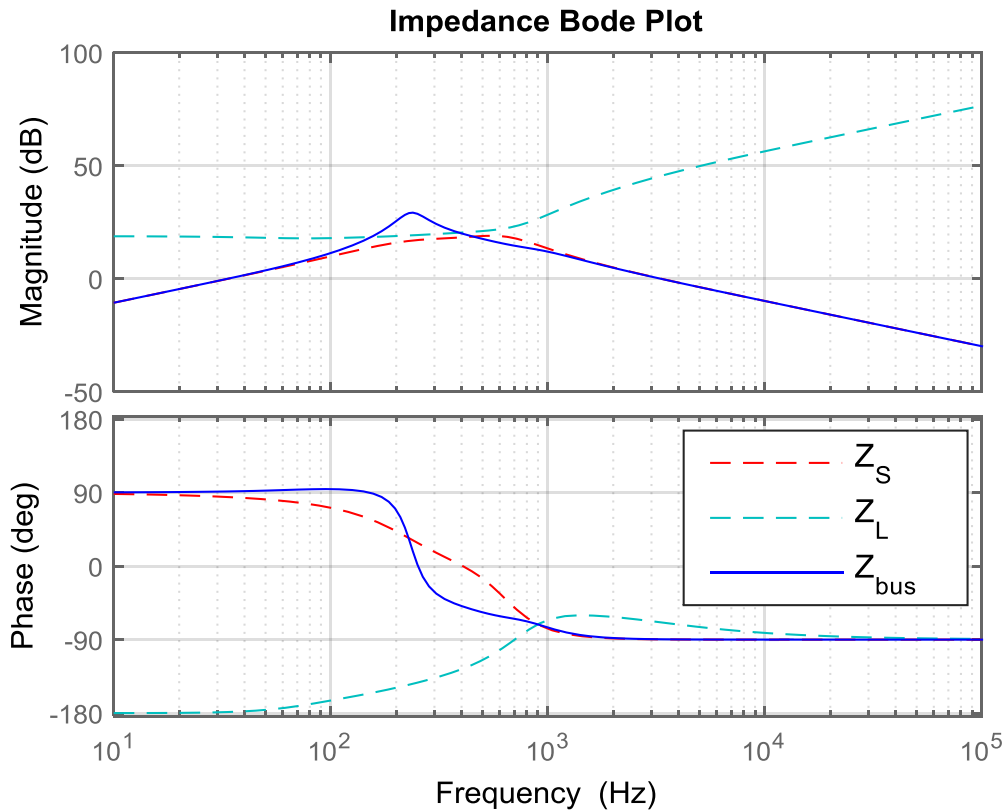


**Figure 2.7. Bus impedance Bode plot.**

The Bode plot of **Figure 2.7** reveals that the bus impedance  $Z_{bus}(s)$  follows the source output impedance everywhere except around the range of frequencies where the source and load impedances are comparable in magnitude.

The resonance peak of  $Z_{bus}(s)$  is at 234 Hz; **Figure 2.8** shows that the bus impedance has a pair of poles at this frequency with low damping factor of  $\zeta = 0.153$ , which also corresponds to a quality factor  $|Q|_{dB} = 10.29 \text{ dB}$ .

Since all poles and zeros are located in the left half plane in the  $s$ -domain, the system is expected to be stable. However, in presence of disturbances, undesirable oscillations might appear.

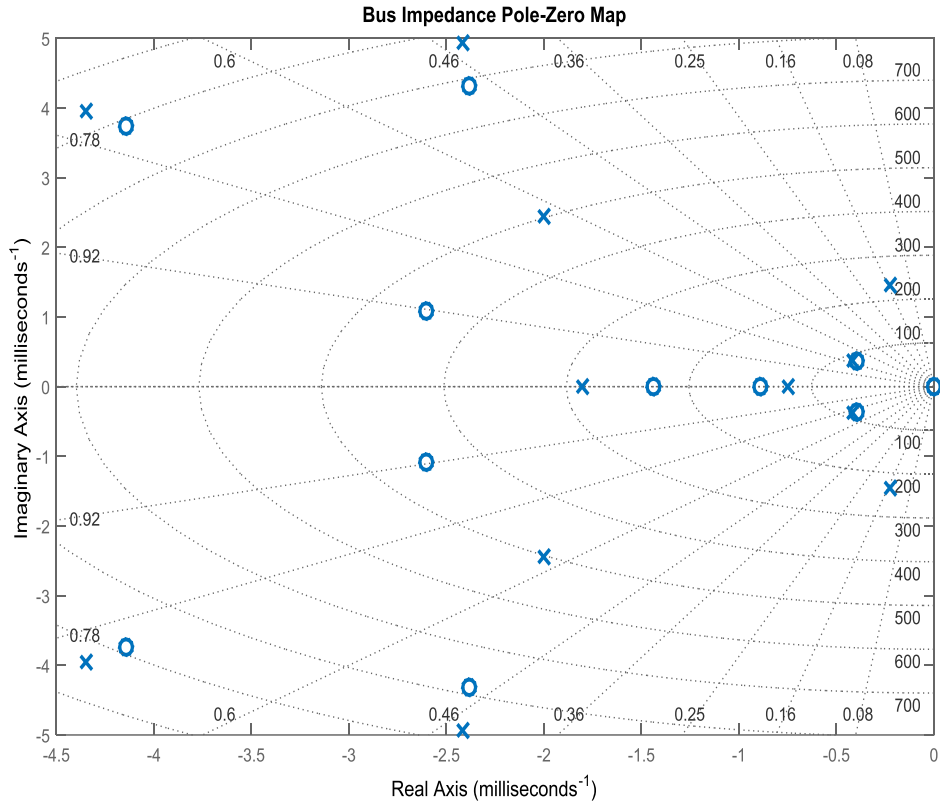


**Figure 2.8. Poles and zeros of the bus impedance.**

This is confirmed by the Nyquist plot in **Figure 2.9**. The Nyquist contour of the minor loop gain  $T_{MLG} = Z_s/Z_L$  does not encircle the  $(-1,0)$  point, which implies stability of the system.

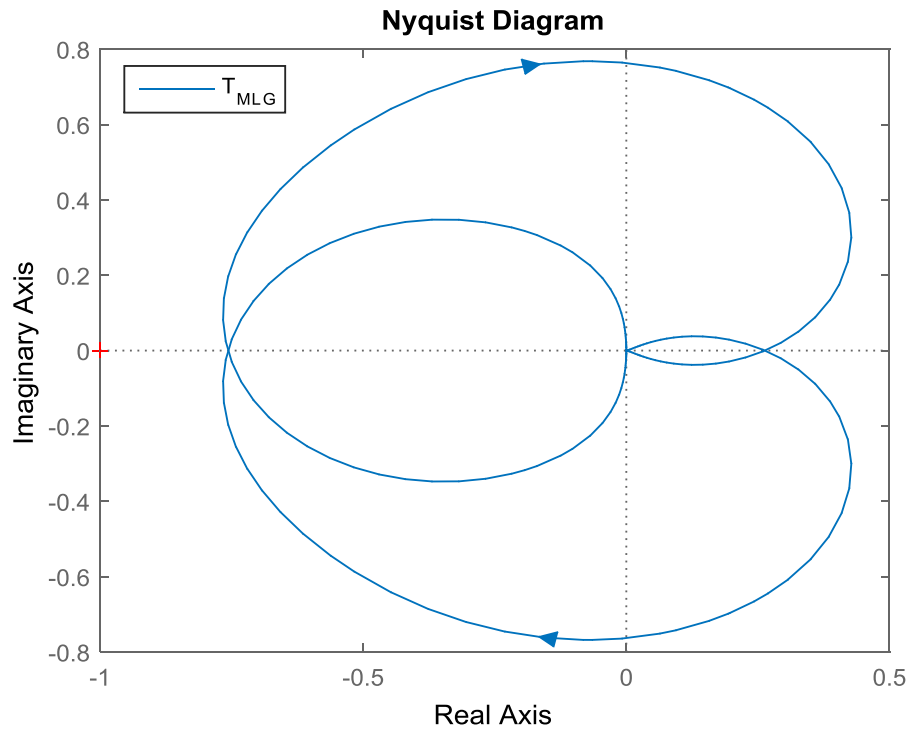


**Figure 2.9.** Nyquist plot of the minor loop gain  $T_{MLG} = Z_s/Z_L$ .

The time domain simulation results in **Figure 2.10** show that oscillations in the system due to a step change in the reference voltage of  $Buck_{LOAD2}$ , from 41.23 V to 45.35 V and then back to 41.23V, are poorly damped.

The next Chapter will discuss the design of Positive Feed-Forward control, to improve system dynamic performance providing a minimum damping factor for bus oscillations.

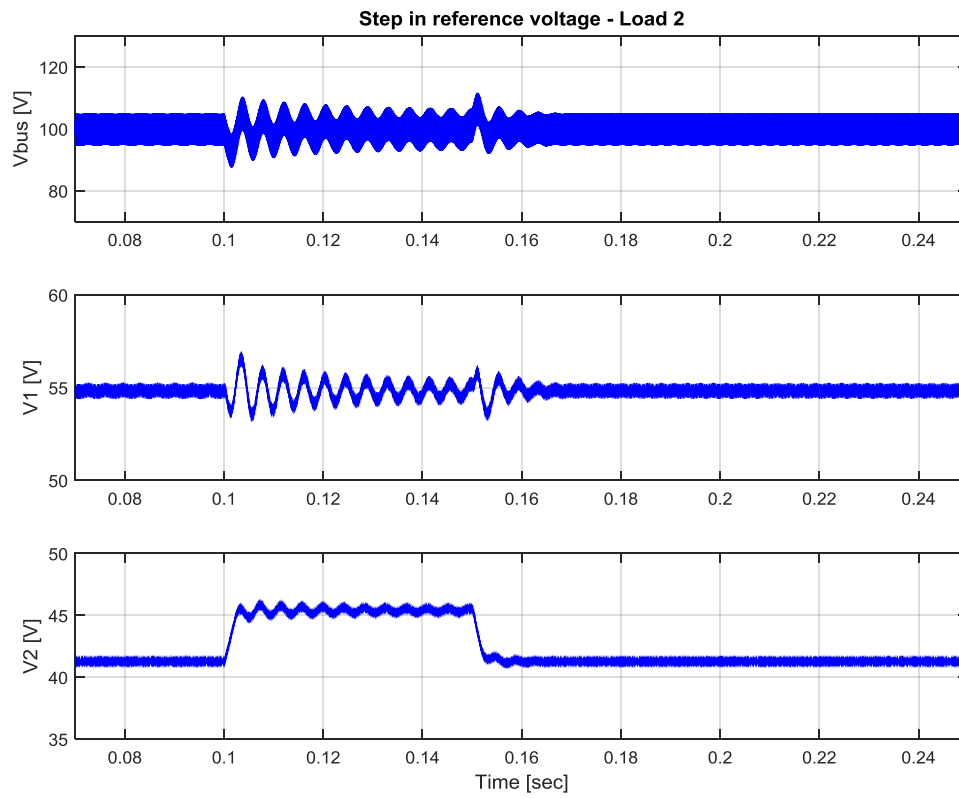


**Figure 2.10.** Time domain simulation results in correspondence with a step in  $V_{2ref}$ .

## CHAPTER 3

### POSITIVE FEED-FORWARD CONTROL

This section introduces the principle of Positive Feed-Forward Control (PFF) and a new approach for the design of the feed-forward gain based on the desired damping for oscillations in DC power distribution system. The approach is validated using frequency domain and time domain simulations results.

#### 3.1. Principle of PFF control

Positive Feed-Forward control is proposed in [8] [9] [10] [11] as an alternative active damping approach to improve the stability of a feedback-controlled switching converter system, which is degraded due to source subsystem interaction.

The scheme is shown in **Figure 3.1**; a positive feed-forward loop is included in combination with the already existing negative feedback for output regulation. The effect of the positive feed-forward loop is the introduction of a virtual damping impedance at the input ports of the converter.

The main advantage of this approach is that it does not require hardware modification of the physical system and it provides the possibility of online tuning for an adaptive control implementation.

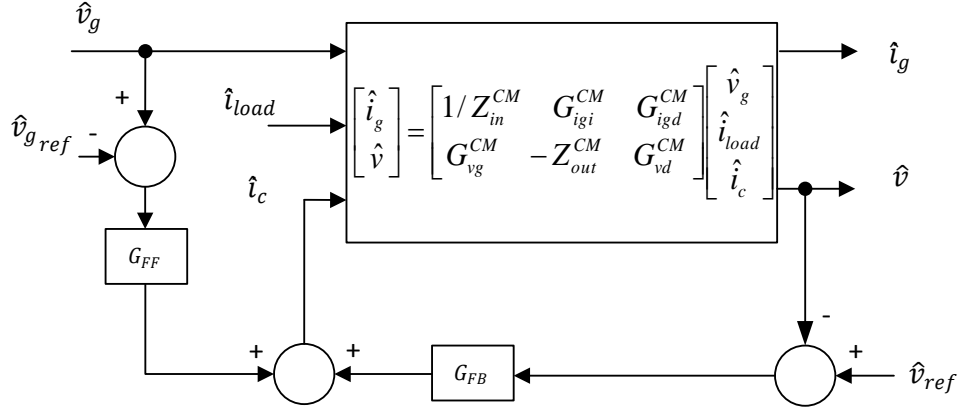


**Figure 3.1. PFF control block diagram.**

Substitution of (3.1) into (2.2) results in the closed loop small-signal model (3.2) for the combined feed-forward and feedback control of **Figure 3.1**.

$$\hat{i}_c = (\hat{v}_g - \hat{v}_{g\_ref}) G_{cFF} + (\hat{v}_{ref} - \hat{v}) G_{cFB} \quad (3.1)$$

$$\begin{bmatrix} \hat{i}_g \\ \hat{v} \end{bmatrix} = \begin{bmatrix} \frac{1}{Z_{in}^{FFFB}} & G_{igi}^{FFFB} & G_{igc1}^{FFFB} & G_{igc2}^{FFFB} \\ G_{vg}^{FFFB} & -Z_{out}^{FFFB} & G_{vc1}^{FFFB} & G_{vc2}^{FFFB} \end{bmatrix} \begin{bmatrix} \hat{v}_g & \hat{i}_{load} & \hat{v}_{ref} & \hat{v}_{g\_ref} \end{bmatrix}^T \quad (3.2)$$

The transfer functions in (3.2) are given by (3.3)-(3.10).

$$\frac{1}{Z_{in}^{FFFB}} = \frac{1}{Z_{in}^{FB}} + \frac{1}{Z_{damp}} \quad (3.3)$$

$$G_{igi}^{FFFB} = G_{igi}^{FB} \quad (3.4)$$

$$G_{igc1}^{FFFB} = G_{igc}^{FB} \quad (3.5)$$

$$G_{igc2}^{FFFB} = -\frac{1}{Z_{damp}} \quad (3.6)$$

$$G_{vg}^{FFFB} = G_{vg}^{FB} + \frac{G_{vc}^{CM}}{G_{igc}^{CM}} \frac{1}{Z_{damp}} \quad (3.7)$$

$$Z_{out}^{FFFB} = Z_{out}^{FB} \quad (3.8)$$

$$G_{vc1}^{FFFB} = G_{vc}^{FB} \quad (3.9)$$

$$G_{vc2}^{FFFB} = -\frac{G_{vc}^{CM}}{G_{igc}^{CM}} \frac{1}{Z_{damp}} \quad (3.10)$$

From equation (3.3) it can be verified that the effect of the positive feed-forward loop is to add a virtual damping impedance at the input port of the converter, in parallel with the existing input impedance under feedback control only. The expression for the damping impedance is given in (3.11), where  $T_{FF}$  is the feed-forward loop given in (3.12).

$$Z_{damp} = \frac{T_{FB} + 1}{T_{FF}} \quad (3.11)$$

$$T_{FF} = G_{C_{FF}} G_{igc_{PI}} \quad (3.12)$$

This virtual impedance can be designed in a way that the overall system meets certain dynamic specifications, like a desired damping factor, and from (3.12) the feed-forward gain  $G_{C_{FF}}$  can be determined for the implementation of PFF control.

There is some trade off that has to be made according to the specific application for which the converter is utilized; equation (3.7) shows that the input-to-output voltage transfer function, also called audio susceptibility, is degraded with the implementation of PFF control.

Summarizing, **Figure 3.2** shows the effects of PFF control on the two port hybrid g-parameter unterminated model developed in the previous chapter. Note that usually  $\hat{v}_{g_{ref}} = 0$ , since the goal of the PFF control is to stabilize the bus voltage.

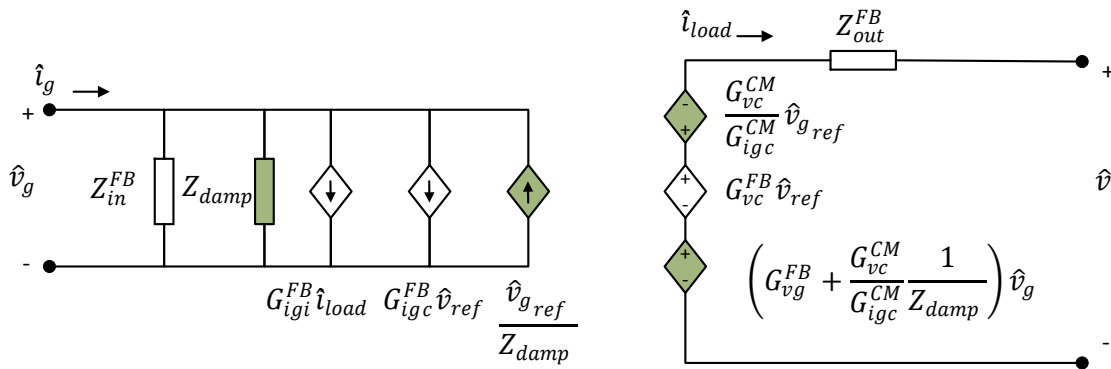


**Figure 3.2. Unterminated small-signal model with PFF control.**

### 3.2. The design of the PFF control

A new approach for the design of PFF control based on the desired dynamic characteristics of the system is presented in this section.

It was shown that the effect of PFF control is to introduce a virtual damping impedance  $Z_{damp}$  at the input port of the converter. **Figure 3.3** (a) is obtained by considering the interacting system of Section 2.2, including the damping impedance and a current injection at the DC bus for estimation of the bus impedance. In **Figure 3.3** (b), the bus impedance  $Z_{bus}$  represents the parallel combination of the source output impedance and the load input impedance under feedback control only.

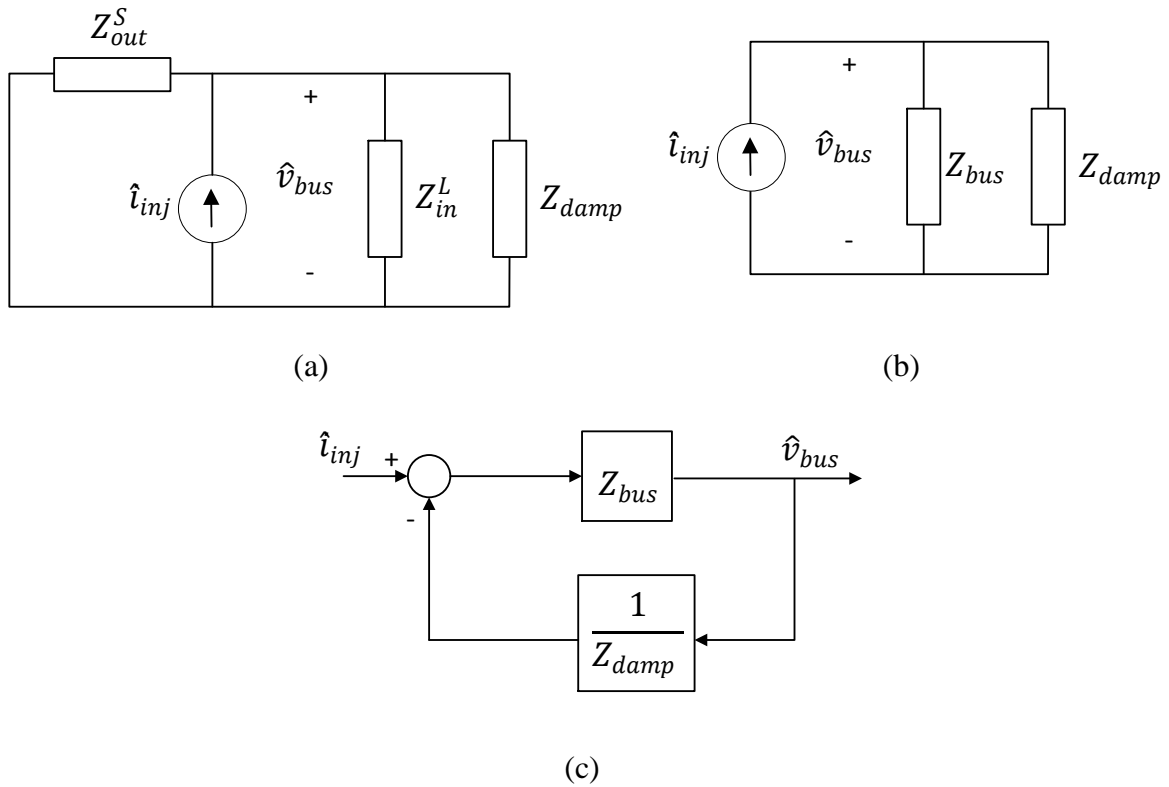


**Figure 3.3. Interacting subsystems representation with PFF control: (a) circuitual model, (b) reduced circuitual model and (c) block diagram.**

The expression for the new overall bus impedance under feedback and feed-forward control is obtained by determining the current injection-to-bus voltage transfer

function given in (3.13), which resembles the closed loop transfer function of a negative feedback control system where the forward gain is the original bus impedance and the feedback gain is the damping admittance, as shown in **Figure 3.3** (c).  $Z_{damp}$  can be designed based on the desired location of the dominant poles of (3.13).

$$Z_{busFF} = \frac{Z_{bus}}{1 + \frac{Z_{bus}}{Z_{damp}}} \quad (3.13)$$

If we wish to have a pair of dominant poles  $s_{r1,2}$  at the resonant frequency  $\omega_{res}$  with minimum damping factor  $\zeta_{min}$ ;  $s_r$  given by (3.14) must satisfy the characteristic equation of (3.13). This can be obtained by imposing the magnitude and phase conditions on (3.15) and (3.16) [17].

$$s_r = -\omega_{res}\zeta_{min} \pm j\omega_{res}\sqrt{1 - \zeta_{min}^2} \quad (3.14)$$

$$\left| \frac{Z_{bus}(s_r)}{Z_{damp}(s_r)} \right| = 1 \quad (3.15)$$

$$\arg\left(\frac{Z_{bus}(s_r)}{Z_{damp}(s_r)}\right) = \pm\pi \quad (3.16)$$

A passive  $R_d - L_d - C_d$  parallel damping will be considered as the desired damping impedance so that the bus impedance is only modified in a certain frequency range around the resonant frequency.

The general expression for the damping impedance in the  $s$ -domain is given in (3.17), where the resonant frequency  $\omega_d$ , the Q-factor and the characteristic impedance  $Z_0$  are the three unknowns.

$$Z_{damp}(s) = R_d + sL_d + \frac{1}{sC_d} = Z_0 \frac{\frac{s^2}{\omega_d^2} + \frac{s}{\omega_d Q_d} + 1}{\frac{s}{\omega_d}} \quad (3.17)$$

$$\omega_d = \frac{1}{\sqrt{L_d C_d}} \quad (3.18)$$

$$Q_d = \frac{1}{R_d} \sqrt{\frac{L_d}{C_d}} \quad (3.19)$$

$$Z_0 = \sqrt{\frac{L_d}{C_d}} = \frac{1}{\omega_d C_d} = \omega_d L_d \quad (3.20)$$

The Q-factor for  $Z_{damp}$  is chosen to be  $Q_d = 0.5$  (damping factor  $\zeta_d = 1$ ) to avoid the appearance of additional resonances, then the expression for  $Z_{damp}$  can be rearrange as in (3.21).

$$Z_{damp}(s) = Z_0 \frac{1 + 2\frac{s}{\omega_d} + \frac{s^2}{\omega_d^2}}{\frac{s}{\omega_d}} = \frac{Z_0}{\omega_d} \frac{(\omega_d + s)^2}{s} \quad (3.21)$$

From the phase condition given in (3.16) the angle in (3.22) is obtained as follows:

$$\begin{aligned}
& \arg(Z_{bus}(s_r)) - \arg(Z_{damp}(s_r)) = \pi \\
& \arg(Z_{bus}(s_r)) - 2\arg(\omega_d + s_r) + \arg(s_r) = \pi \\
& \varphi = \arg(\omega_d + s_r) = \frac{\arg(Z_{bus}(s_r)) + \arg(s_r) - \pi}{2}
\end{aligned} \tag{3.22}$$

Also,

$$\varphi = \arg(\omega_d + s_r) = \tan^{-1} \left( \frac{\omega_{res} \sqrt{1 - \zeta_{min}^2}}{\omega_d - \omega_{res} \zeta_{min}} \right) \tag{3.23}$$

Combining (3.22) and (3.23), the frequency  $\omega_d$  is obtained.

$$\omega_d = \zeta_{min} \omega_{res} + \frac{\omega_{res} \sqrt{1 - \zeta_{min}^2}}{\tan \varphi} \tag{3.24}$$

From the amplitude condition in (3.15) the value of  $Z_0$  is found to be:

$$\begin{aligned}
Z_0 &= \omega_d \frac{|Z_{bus}(s_r)| |s_r|}{|\omega_d + s_r|^2} \\
&= \frac{\omega_d \omega_{res}}{\omega_d^2 + \omega_{res}^2 - 2\omega_d \omega_{res} \zeta_{min}} |Z_{bus}(s_r)|
\end{aligned} \tag{3.25}$$

The inductance  $L_d$ , capacitance  $C_d$  and resistance  $R_d$  are then determined as:

$$L_d = \frac{Z_0}{\omega_d} \quad C_d = \frac{1}{L_d \omega_d^2} \quad R_d = \frac{Z_0}{Q_d} \tag{3.26}$$

### 3.3. An illustrative example and simulation

In this section, the proposed method will be utilized to improve the damping of the DC system introduced in Section 2.3, in which  $Buck_{SOURCE}$  regulates the DC bus voltage and  $Buck_{LOAD1}$  and  $Buck_{LOAD2}$  feed resistive loads at different voltage levels.

The design procedure starts with the choice of the desired location of the dominant poles of the bus impedance; considering that the minimum damping factor  $\zeta_{min} = 0.5$  is desired at the resonant frequency  $\omega_{res} = 234 \text{ Hz}$ , the corresponding desired dominant poles given by (3.14) are:

$$s_r = 2\pi \times 234 \text{ Hz} \left[ -0.5 \pm j \frac{\sqrt{3}}{2} \right] \quad (3.27)$$

The magnitude and phase of the bus impedance evaluated at  $s_r$  are:

$$\begin{aligned} |Z_{bus}(s_r)| &= 10.13 \Omega \\ \arg(Z_{bus}(s_r)) &= 219.34^\circ \end{aligned} \quad (3.28)$$

From the conditions (3.15) and (3.16), the magnitude and the phase of the damping impedance must be:

$$\begin{aligned} |Z_{damp}(s_r)| &= |Z_{bus}(s_r)| = 10.13 \Omega \\ \arg(Z_{damp}(s_r)) &= \arg(Z_{bus}(s_r)) - 180^\circ = 39.34^\circ \end{aligned} \quad (3.29)$$

And from equations (3.23) to (3.26) the components of the parallel damping impedance are found to be:

$$R_d = 17.2\Omega \quad L_d = 9mH \quad C_d = 120\mu F \quad (3.30)$$

**Figure 3.4** shows the new bus impedance when PFF control is implemented on  $Buck_{LOAD1}$ . Compared to the original bus impedance the resonant peak is reduced. The dominant poles at 234 Hz have damping factor  $\zeta_{min} = 0.5$ , as shown in **Figure 3.5**.

With the addition of the PFF control, the number of zeros and poles of the bus impedance is increased by two, due to the zeros of the added damping impedance.

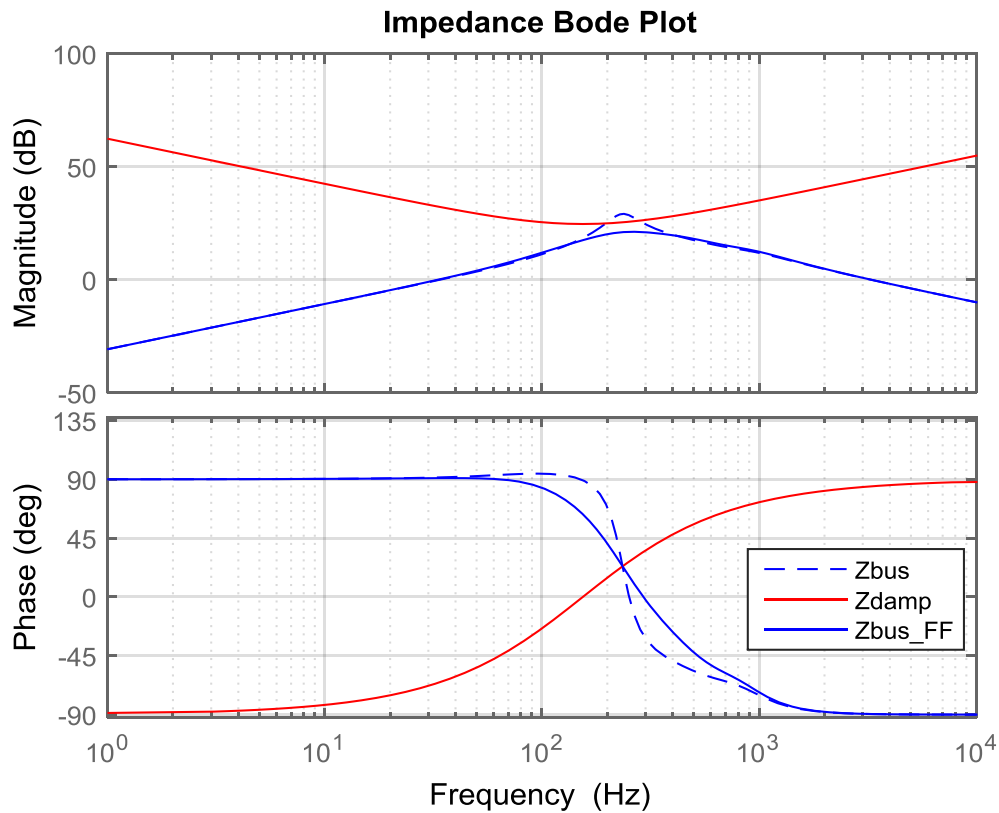


**Figure 3.4. Bus impedance Bode plot, with PFF control.**

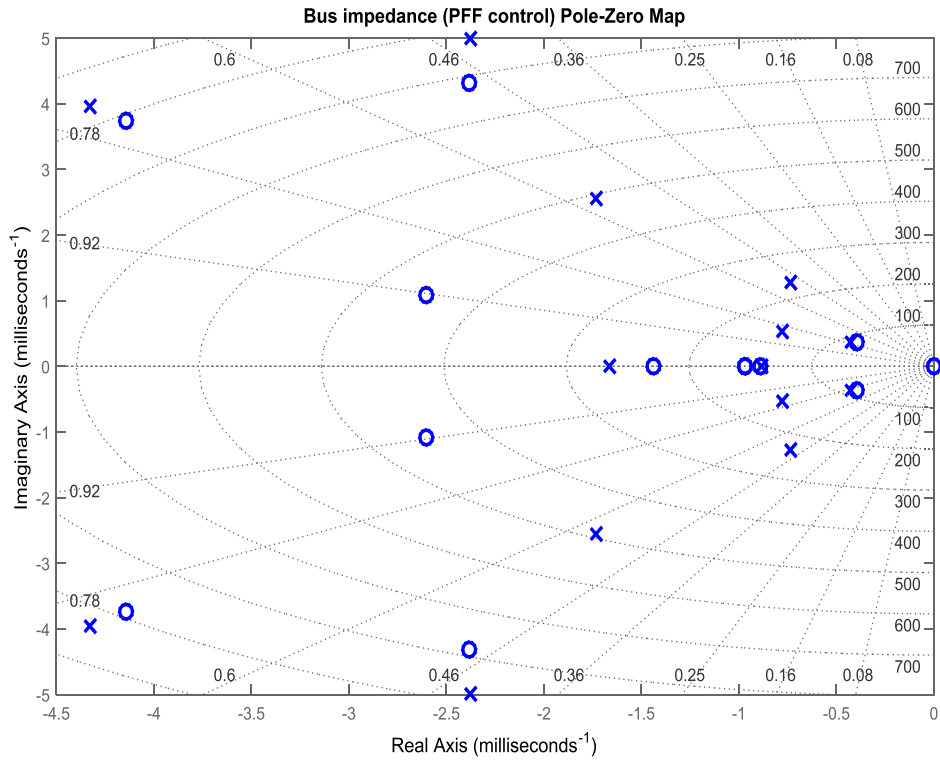


**Figure 3.5. Poles and zeros of the bus impedance, with PFF control.**

The time domain simulation results, in **Figure 3.6**, show the improvement on the damping factor of the DC system, significantly reducing the oscillations after a step change in the reference voltage of *Buck<sub>LOAD2</sub>*.

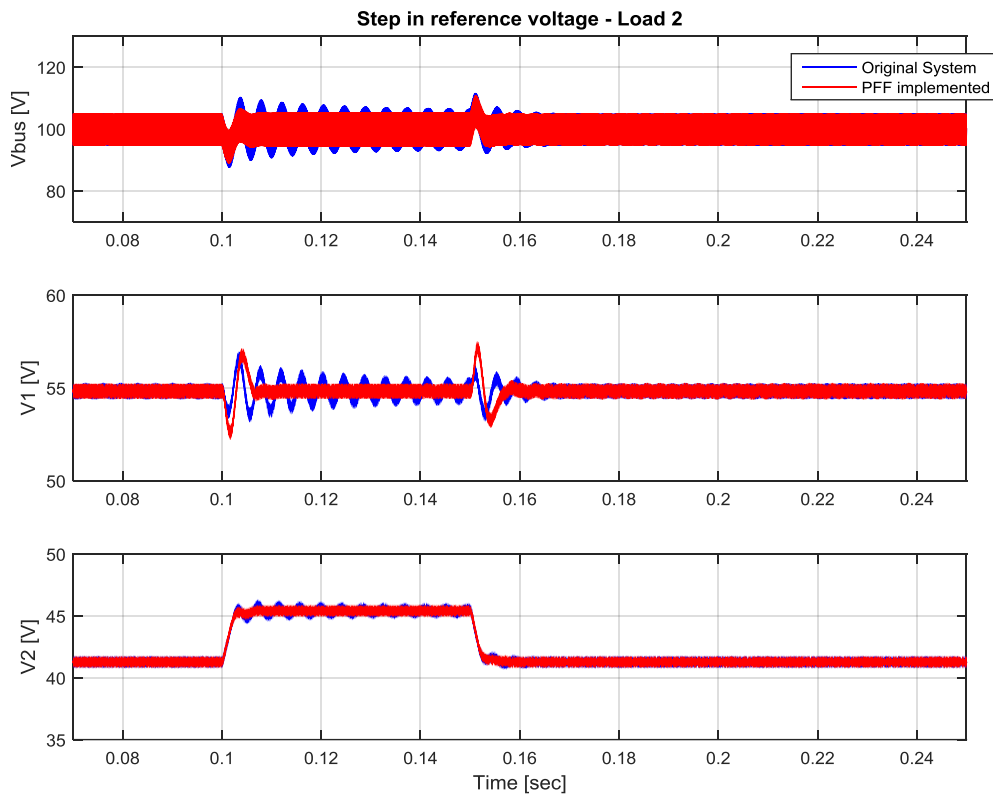


**Figure 3.6. Improvement in the time domain simulation results with PFF control.**

As it was stated previously, the tradeoff in the application of Positive Feed-Forward control is that the input-to-output voltage transfer function is degraded at low frequency, as shown in **Figure 3.7**.

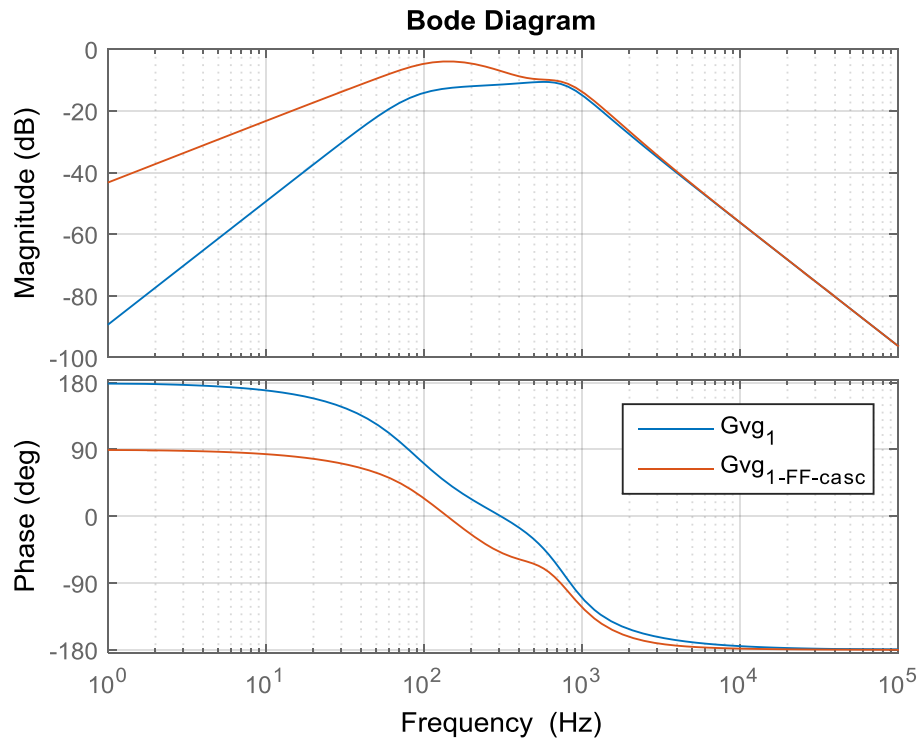


**Figure 3.7. Bode plot of the input voltage-to-output voltage transfer function.**

Another important aspect of cascaded systems is the degradation of the feedback loop gain shown in **Figure 3.8** and **Figure 3.9**, which affects the output performance of the converters. It can be noticed that Positive Feed-Forward control also has a negative effect on the loop gain reducing the phase margin for which the voltage feedback control was designed originally.

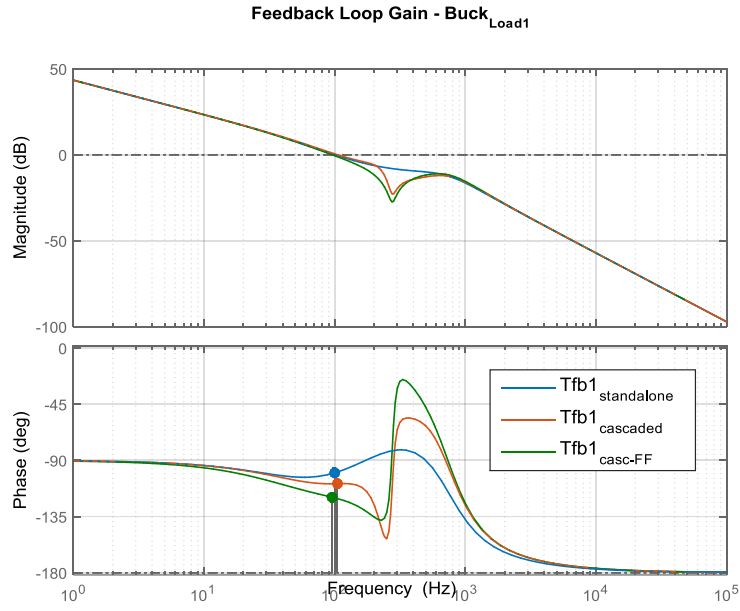


**Figure 3.8. Feedback loop gain of  $Buck_{LOAD1}$ .**

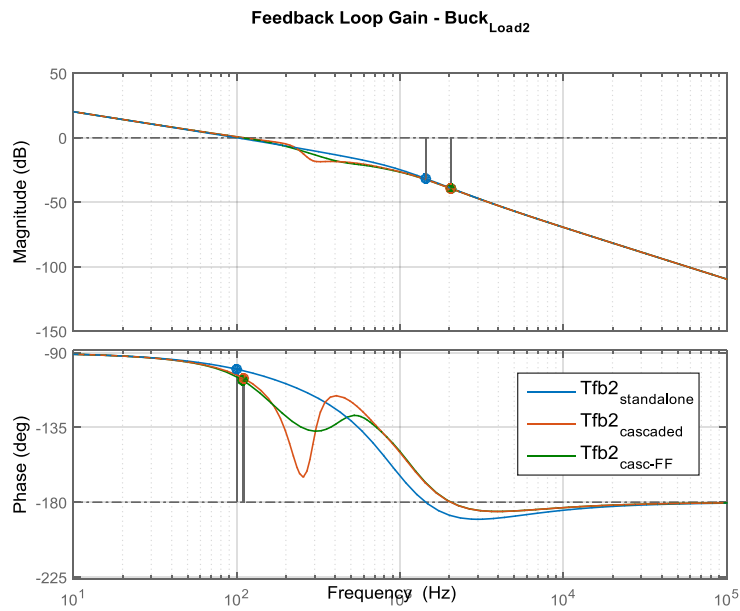


**Figure 3.9. Feedback loop gain of  $Buck_{LOAD2}$ .**

### 3.4. A decentralized implementation of PFF control

In the previous example, PFF control is implemented in  $Buck_{LOAD1}$  improving the damping of the system. In this section a decentralized implementation will be considered; the objective is to obtain more reliability for the system taking into consideration the possibility of load shedding or system reconfiguration.

Considering an operating condition that requires the disconnection of  $Buck_{LOAD1}$ , the dynamic characteristics of the remaining system will be affected by the loss of PFF control and consequently the virtual damping impedance. If no actions are taken while  $Buck_{LOAD1}$  is offline, the dominant poles of the overall impedance will have a damping factor of 0.26 as is shown in **Figure 3.10** (blue).

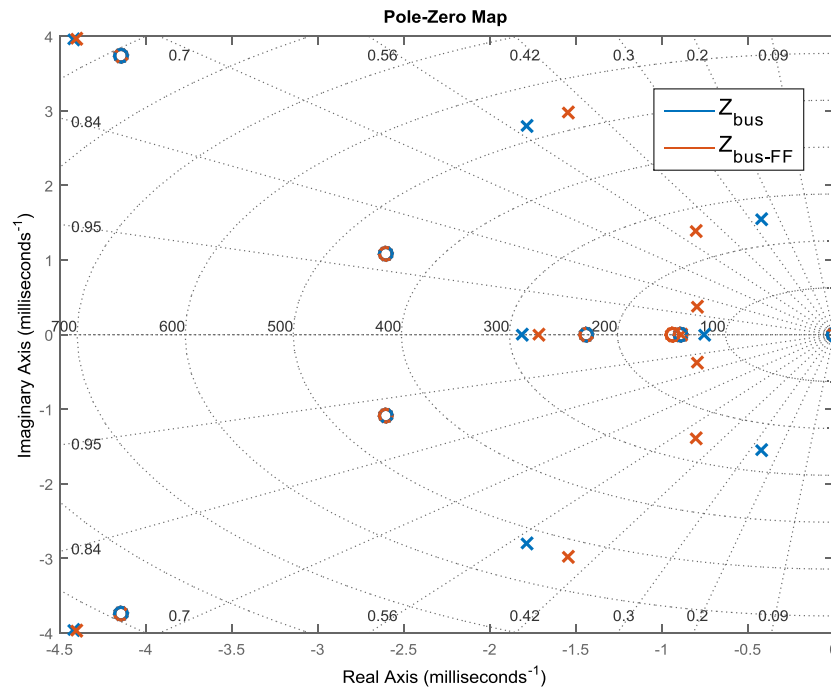


**Figure 3.10. Poles and zeros of the bus impedance under FB control (blue) and FFFB (red).**

For the remaining system, the required damping impedance that will maintain the minimum damping factor of 0.5, can be found following the closed-form design procedure proposed in the previous section. The parameters of the parallel damping impedance are found to be:

$$R_{d2} = 23.84\Omega \quad L_{d2} = 12.72mH \quad C_{d2} = 89.52\mu F$$

By transferring the PFF control to  $Buck_{LOAD2}$  with the updated feed-forward gain, the dominant poles of the overall bus impedance are moved farther away from the imaginary axis, achieving a damping factor of 0.5 at the resonant frequency. The improvement in the location of the dominant poles can be verified in **Figure 3.10** and the effect on the resonant peak of the bus impedance is shown in **Figure 3.11**.

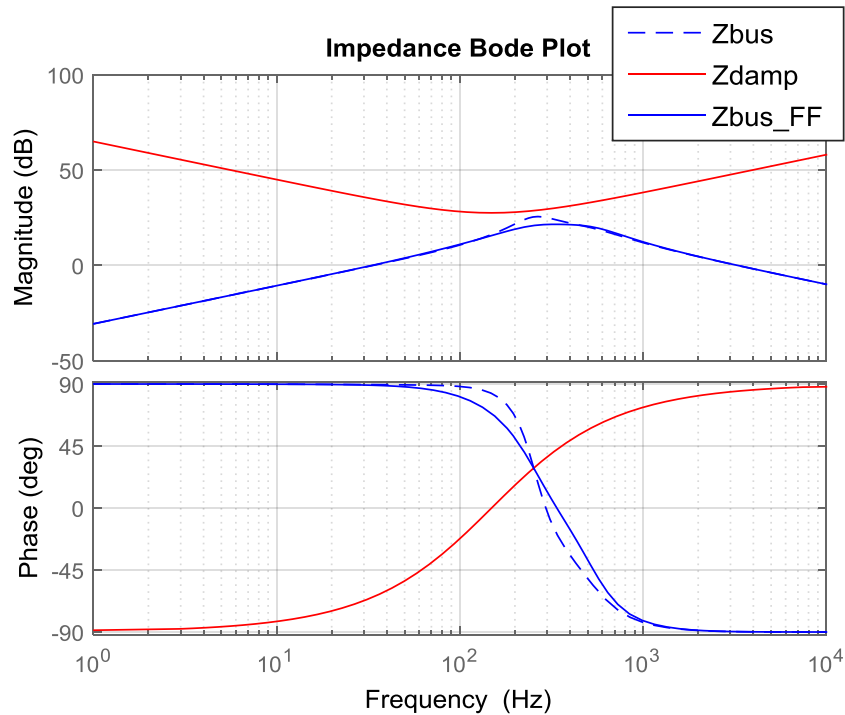


**Figure 3.11. Bus impedance under PFF control.**

**Figure 3.12** shows time domain simulation results; a step change in the reference voltage of  $B_{uckLOAD2}$  is applied for three different scenarios:

- a)  $B_{uckLOAD1}$  and  $B_{uckLOAD2}$  in service and the PFF control is implemented in  $B_{uckLOAD1}$
- b)  $B_{uckLOAD1}$  is out of service and no PFF control is implemented in the remaining system
- c)  $B_{uckLOAD1}$  is out of service and the PFF control is transferred from  $B_{uckLOAD1}$  to  $B_{uckLOAD2}$ .

From this result, it is evident that an adaptive implementation of the PFF control based on the most updated model of the system guarantees that the dynamic performance will remain as specified.

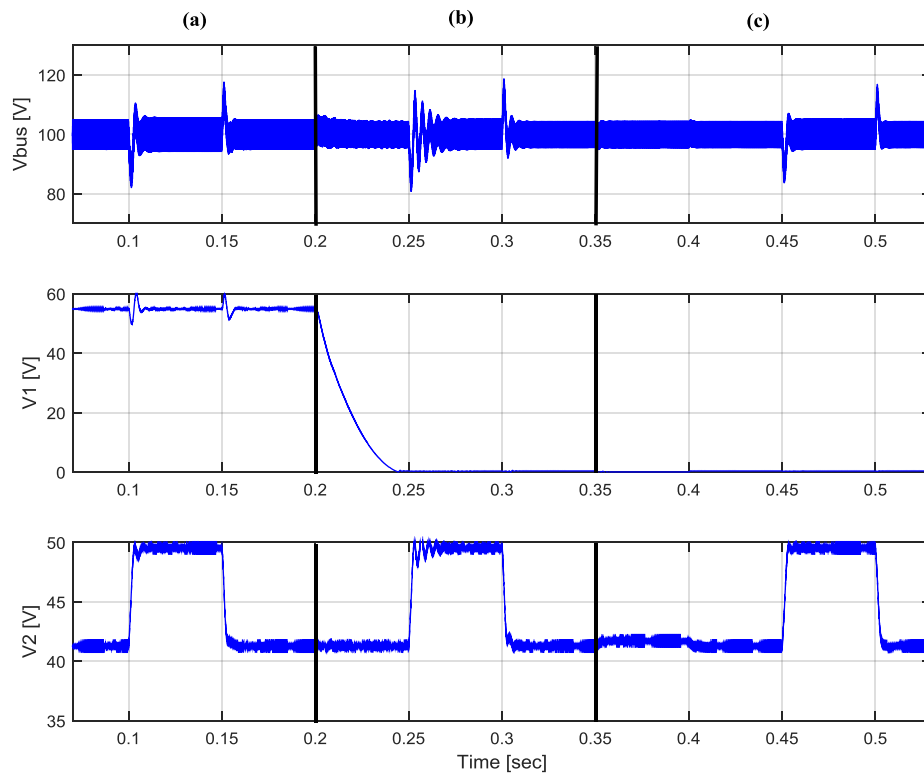


**Figure 3.12.** Time domain simulation results for scenarios (a), (b) and (c).

## CHAPTER 4

### SYSTEM IDENTIFICATION

System identification is a very powerful technique that allows on-line estimation of systems' parameters; in particular we are interested in obtaining input/output impedances of power converters connected to a specific DC bus and the overall bus impedance for stability analysis purposes. In the following chapter a review of the state of the art for wideband impedance identification is presented, followed by a proposed method to improve the estimation accuracy and a technique to obtain the bus impedance performing local measurements on each converter.

#### 4.1. Cross-correlation method

In this section we review the cross-correlation method which measures the similarity between two signals [18] and that has been applied for system identification of power converters with digital control to estimate control-to-output transfer functions [19] [20] [21] [14] and network impedances [12] [13].

In steady-state for small signal disturbances, a digitally controlled power converter can be considered as a linear time-invariant discrete-time system, where the sampled system is represented as:

$$y[n] = \sum_{k=1}^{\infty} h[k]u[n - k] + v[n] \tag{4.1}$$

In (4.1)  $y[n]$  is the sampled output signal,  $u[n]$  the input digital control signal,  $h[n]$  is the discrete-time system impulse response and  $v[n]$  represents disturbances such as switching noise, measurement error, quantization noise, etc. as shown in **Figure 4.1**.

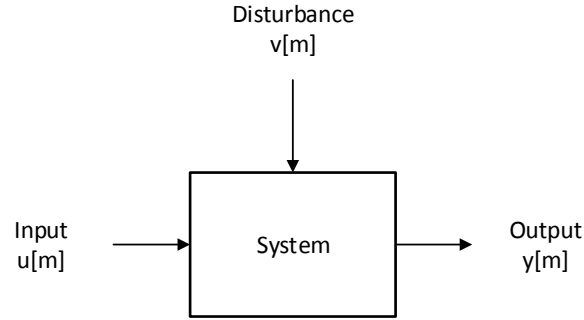


**Figure 4.1. Linear time-invariant system**

The cross-correlation of the input and output signals is:

$$\begin{aligned}
 R_{uy}[m] &= \sum_{n=1}^{\infty} u[n]y[n+m] \\
 &= \sum_{n=1}^{\infty} h[n]R_{uu}[m-n] + R_{uv}[m]
 \end{aligned}
 \tag{4.2}$$

where  $R_{uu}[m]$  is the auto-correlation of the input signal and  $R_{uv}[m]$  is the input-to-disturbance cross-correlation.

The relations in (4.3) hold when white noise is used as input, which is a random signal with constant power spectral density.

$$\begin{cases} R_{uu}[m] = \delta[m] \\ R_{uv}[m] = 0 \end{cases} \quad (4.3)$$

It follows that ideally the auto-correlation of the input is a delta function and the cross-correlation of white noise input with disturbances is zero. Under these conditions (4.2) reduces to (4.4) and the cross-correlation of the input and output signals gives the discrete time system impulse response.

$$R_{uy}[m] = h[m] \quad (4.4)$$

The input to output transfer function in the frequency domain can be derived by applying Discrete Fourier Transform (DFT). For a given finite-duration sequence  $x[n]$  of length  $N$ , so that  $x[n] = 0$  for  $n < 0$  and  $n \geq N$ , the DFT is defined as in (4.5).

$$X(k) = \sum_{n=0}^{N-1} x[n] e^{-j2\pi kn/N}, \quad k = 0, 1, \dots, N-1 \quad (4.5)$$

So the input-to-output transfer function can be found from (4.6).

$$H(k) = DFT\{R_{uy}[m]\} = \sum_{n=0}^{N-1} R_{uy}[n] e^{-j2\pi kn/N}, \quad k = 0, 1, \dots, N-1 \quad (4.6)$$

#### 4.2. Maximum length Pseudo-Random Binary Sequences (PRBS)

The analysis above requires the use of white noise as input perturbation. An infinite-bandwidth white noise signal is a purely theoretical construction and the bandwidth is limited in practice by the mechanism of noise generation. A random signal

is considered white noise if it presents a flat spectrum over the range of frequencies of interest.

In this context an approximation of white noise can be accomplished in digitally controlled converters by using a maximum length Pseudo Random Binary Sequence (PRBS) signal as input perturbation.

A PRBS signal is a series of width modulated rectangular pulses as shown in **Figure 4.2**. This signal, while appearing random, is in fact a periodic and deterministic signal, which implies that the sequence can be repeated and its output can be determined when the initial conditions and the sequence generation scheme are specified.

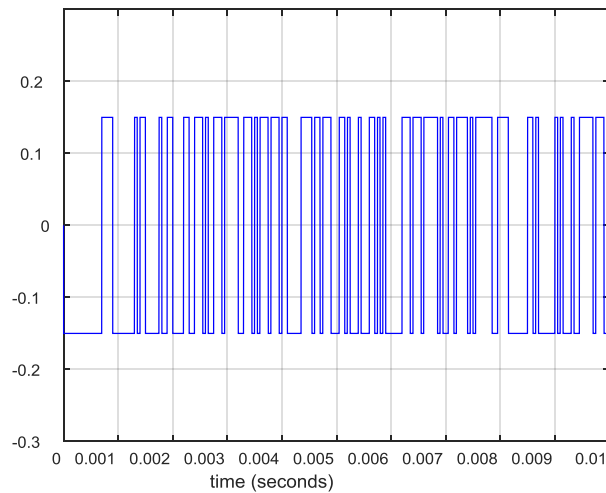


**Figure 4.2. PRBS signal**

The PRBS signal can be generated by a shift register with feedback. The two variables that have to be defined in the generation of a maximum length PRBS signal are the period length, determined by the number of shift register bits, and the frequency band which depends on the sequence length and the sample frequency.

An N-bit register will generate a PRBS of length  $L$  given in (4.7), the lower and upper limits of the bandwidth are given in (4.8), where  $T$  is the clock period of the shift register and  $f_s$  is the converter switching frequency.

$$L = 2^N - 1 \tag{4.7}$$

$$\begin{cases} f_{lower} = \frac{1}{L \times T} \\ f_{upper} = \frac{f_s}{2} \end{cases} \tag{4.8}$$

A given power converter cannot be controlled beyond the Nyquist frequency, which is half of the switching frequency  $f_s$ ; it follows that, in order to obtain the highest possible bandwidth, the bit period has to be chosen equal to the inverse of  $f_s$  as in (4.9).

$$T = \frac{1}{f_s} \tag{4.9}$$

#### 4.3. Simplifications of the cross-correlation method

In order to save time domain cross-correlation calculations, simplifications to the existing methodology are proposed in [22] so that almost all calculations are made in the frequency domain.

Given two sequences  $\{x_1[n]\}$  and  $\{x_2[n]\}$  of length N, with DFT given in (4.10) and (4.11). From the properties of the DFT it is known that the product of  $X_1(k)$  and  $X_2(k)$  is equivalent to the DFT of the circular convolution of the two sequences in the time domain as shown in (4.12) [18].

$$X_1(k) = \sum_{n=0}^{N-1} x_1[n] e^{-\frac{j2\pi nk}{N}}, \quad k = 0, 1, \dots, N-1$$
(4.10)

$$X_2(k) = \sum_{n=0}^{N-1} x_2[n] e^{-\frac{j2\pi nk}{N}}, \quad k = 0, 1, \dots, N-1$$
(4.11)

$$X_3(k) = X_1(k)X_2(k) \rightarrow x_3[m] = \sum_{n=0}^{N-1} x_1[n]x_2[m-n]_N, \quad m = 0, 1, \dots, N-1$$
(4.12)

This property can be applied to the results in (4.4) and (4.6); so that when the input is white noise (4.14) is obtained.

$$DFT\{R_{uy}[m]\} = DFT\{u[n]\}DFT\{y[n]\}$$
(4.13)

$$H(k) = DFT\{u[n]\}DFT\{y[n]\}$$
(4.14)

The circularity that arises from the property (4.12) eliminates the necessity of padding the sampled data with zeros; which was previously done by applying a Gaussian window [21]. Also, by utilizing the Fast Fourier Transform (FFT) method the required computational calculations can be reduced significantly.

When the desired result is the impedance looking outwards from a power converter as impedance  $Z$  in **Figure 4.3**, the simplification in (4.15) can be made so that the input excitation cancels out and by taking the ratio of the voltage and current DFTs a finite set of values of  $Z(j\omega)$  can be found.

$$Z(j\omega) = \frac{G_{uv}(j\omega)}{G_{ui}(j\omega)} = \frac{DFT\{u[n]\}DFT\{v[n]\}}{DFT\{u[n]\}DFT\{i[n]\}} = \frac{DFT\{v[n]\}}{DFT\{i[n]\}} \quad (4.15)$$

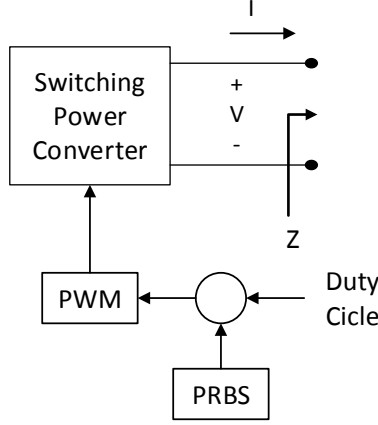


**Figure 4.3. Impedance measurement**

Additionally, when a non-ideal white noise is used to excite the system, from (4.2) it is possible to find the input-to-output transfer function as in (4.16).

$$G_{uy}(j\omega) = \frac{DFT\{R_{uy}[n]\}}{DFT\{R_{uu}[n]\}} = \frac{DFT\{y[n]\}}{DFT\{u[n]\}} \quad (4.16)$$

This reduces the non-ideality introduced by the use of PRBS signal as an approximation of white noise and also corrects the results for colored noise if used instead of white noise.

#### 4.4. On-line impedance estimation using a double PRBS signal injection

In previous works [12] [13] [21], the injection of the PRBS signal was done as shown in **Figure 4.4** in order to directly perturb the duty cycle signal. The impedance

looking out from the converter can then be obtained from (4.15) by measuring the corresponding voltages and currents.

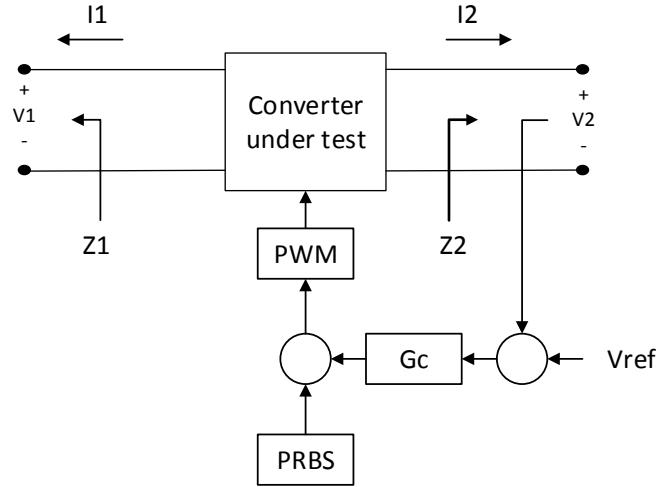


**Figure 4.4. Single PRBS injection in the duty cycle signal for impedance estimation**

In case of feedback-controlled converters like in **Figure 4.4**, the perturbation is attenuated at low frequencies by the factor  $1/T(s)$ , where  $T(s)$  represents the feedback loop gain of the converter under test. As an example, the effect of the feedback in the perturbation-to-output voltage transfer function is given in (4.17).

$$\frac{\hat{v}_2}{PRBS} = \frac{G_{vd}}{1 + T(j\omega)} \approx \begin{cases} \frac{G_{vd}}{T(j\omega)} & \text{at low frequencies where } |T(j\omega)| \gg 1 \\ G_{vd} & \text{at high frequencies where } |T(j\omega)| \ll 1 \end{cases} \quad (4.17)$$

The feedback attenuates the disturbance introduced by the PRBS signal at low frequencies, where the loop gain is large.

If on the other hand, the perturbation is applied in the reference signal of the FB loop like in **Figure 4.5**, the low frequency identification is expected to be more accurate. However, the signal gets attenuated at higher frequencies by the loop gain  $T(s)$ . The effect of the feedback in the perturbation-to-output voltage transfer function for this case is given in.(4.18).

$$\frac{\hat{v}_2}{PRBS} = \frac{T(j\omega)}{1 + T(j\omega)} \approx \begin{cases} 1 & \text{at low frequencies where } |T(j\omega)| \gg 1 \\ T(j\omega) & \text{at high frequencies where } |T(j\omega)| \ll 1 \end{cases} \quad (4.18)$$

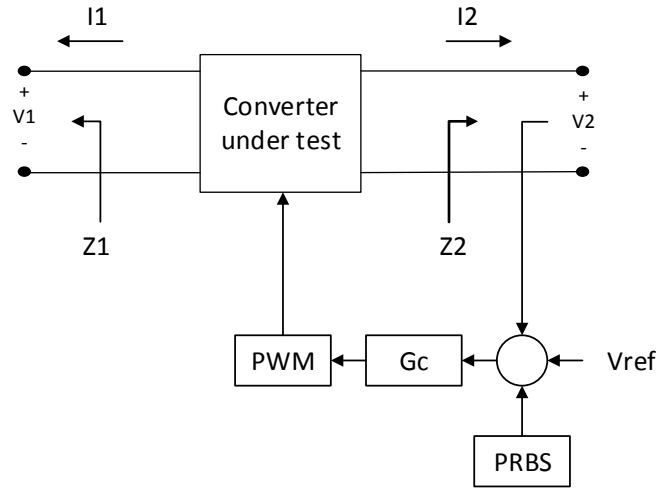


**Figure 4.5. Single PRBS injection in the FB reference signal for impedance estimation**

Since the input/output impedances of power converters vary across the frequency range of operation, it is important to obtain an accurate estimation both at low and high frequencies.

In order to improve the wideband impedance identification, a double injection of the PRBS signal as shown in **Figure 4.6** is proposed.  $K_1$  and  $K_2$  are proper gains to ensure that the amplitude of the perturbations on the one hand is not too small and on the

other hand it does not causes that voltage and current levels exceed 10% of their nominal values in order to avoid large disturbances. In this configuration the perturbation applied to the reference signal dominates at low frequencies, while the perturbation applied to the duty cycle signal dominates at higher frequencies.

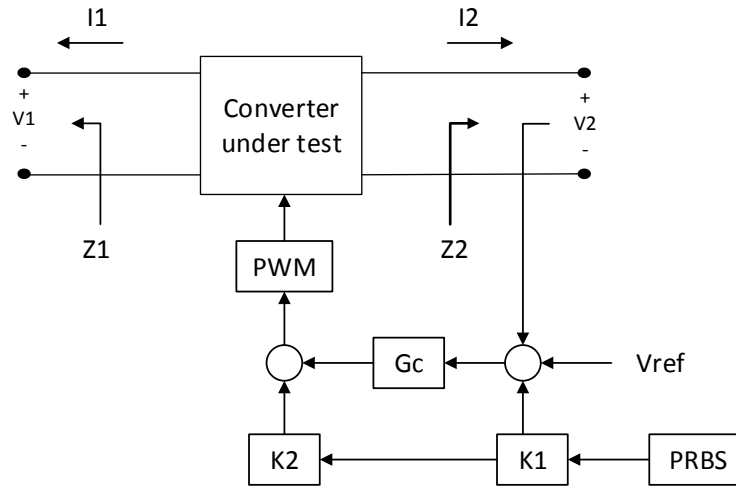


**Figure 4.6. Double injection of the PRBS signal for impedance estimation**

#### 4.5. An illustrative example and simulation

A 14-bit PRBS signal is used to perform impedance identification in the system introduced in Section 2.3; the signal has period  $T = 0.05$  ms which is also the switching period of the converters.

The upper and lower frequency limits can be obtained as shown in Section 4.2:

$$N = 14 \text{ bits}$$

$$L = 2^N - 1 = 16383$$

$$f_{\text{lower}} = \frac{20 \text{ kHz}}{L} = 1.22 \text{ Hz}$$

$$f_{\text{upper}} = f_N = 10 \text{ kHz}$$

One of the difficulties in estimating the impedances is that for certain converters the bus current is a discontinuous signal that changes in amplitude and is also modulated, as shown in **Figure 4.7**. The change in the modulation is problematic, because the sampling should be fast enough to capture the perturbations induced by the injection of the PRBS.

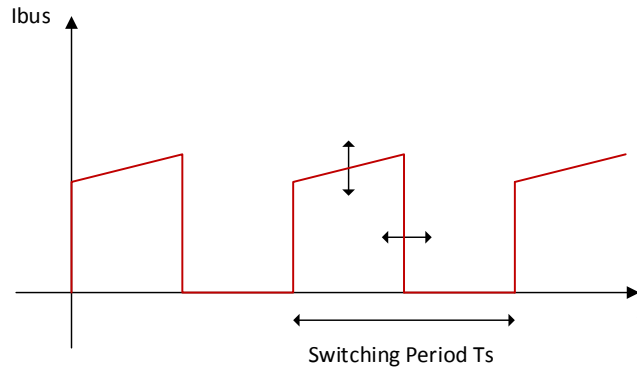


**Figure 4.7. Bus current waveform**

In simulation it is possible to sample at a high rate but in practice this is limited by the capability of Analog-to-Digital Converters (ADC). The sampling frequency of the bus voltage and current signals is chosen to be  $f_{\text{sample}} = 2 \text{ MHz}$ , so that 100 points are obtained in each switching period.

In order to avoid aliasing effect an analog filter is also included to attenuate high frequency noise above the Nyquist frequency.

To build the bus impedance of the DC system introduced in Section 2.3 using the existing power converters, it is necessary to make a test on each converter and measure

the impedance of the equivalent network seen from the converter under test. The three cases are depicted in **Figure 4.8**, **Figure 4.9** and **Figure 4.10**; these tests have the advantage that in each case, the measurements can be done locally in the converter under test.

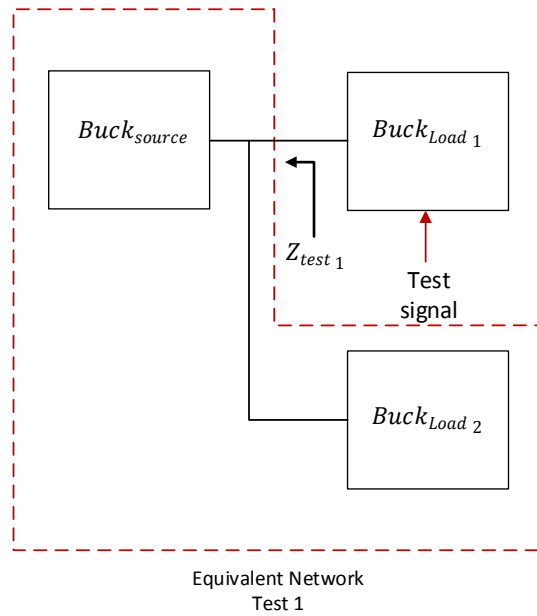


**Figure 4.8. Schematic representation of Test 1**

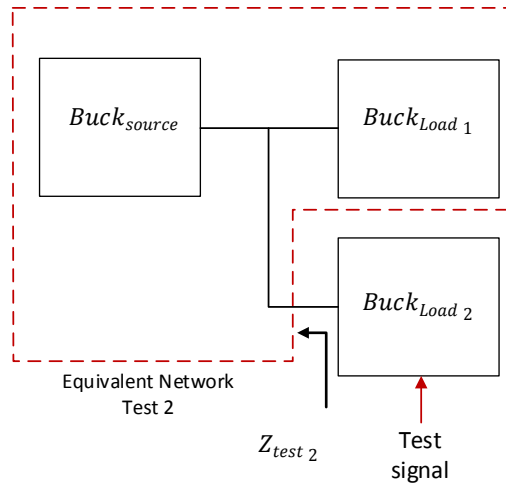


**Figure 4.9. Schematic representation of Test 2**

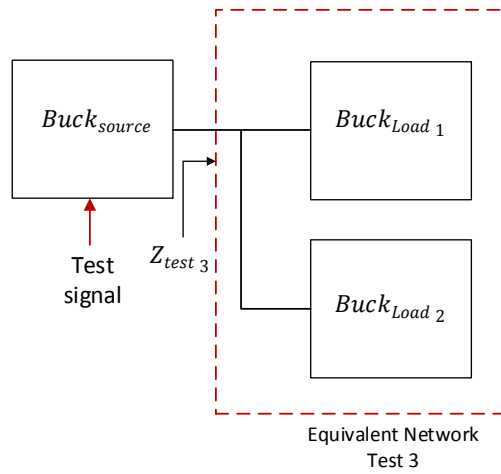


**Figure 4.10. Schematic representation of Test 3**

The measured impedances are given in (4.19)-(4.21).

$$\frac{1}{Z_{test1}} = \frac{1}{Z_{out}^S} + \frac{1}{Z_{in T}^{L2}}$$

(4.19)

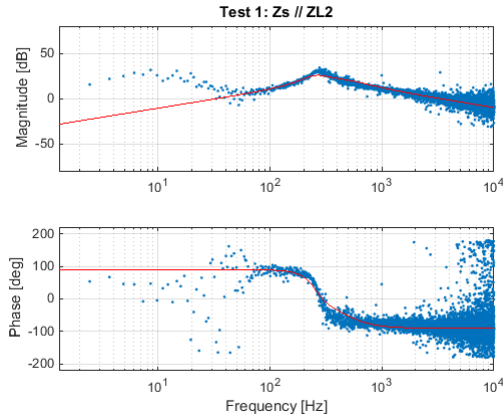
$$\frac{1}{Z_{test_2}} = \frac{1}{Z_{out}^S} + \frac{1}{Z_{in_T}^{L1}} \quad (4.20)$$

$$\frac{1}{Z_{test_3}} = \frac{1}{Z_{in_T}^{L1}} + \frac{1}{Z_{in_T}^{L2}} \quad (4.21)$$

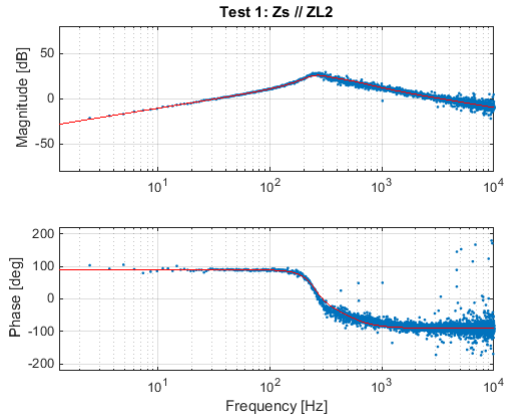
The bus impedance can now be estimated from the parametric models as in (4.22), which can be used in the design of the Positive Feed-Forward Control.

$$\frac{1}{Z_{bus}} = \frac{1}{2} \left[ \frac{1}{Z_{test_1}} + \frac{1}{Z_{test_2}} + \frac{1}{Z_{test_3}} \right] \quad (4.22)$$

The impedance identification results from Test 1, Test 2 and Test 3 are shown in **Figure 4.11**, **Figure 4.12** and **Figure 4.13** respectively, in which the results for single and double injection of the PRBS signal are compared to the analytic impedance transfer functions, presenting improvement in the accuracy especially at low frequencies as expected.

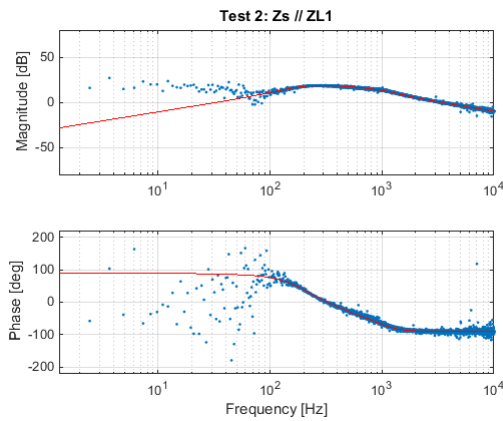


(a)

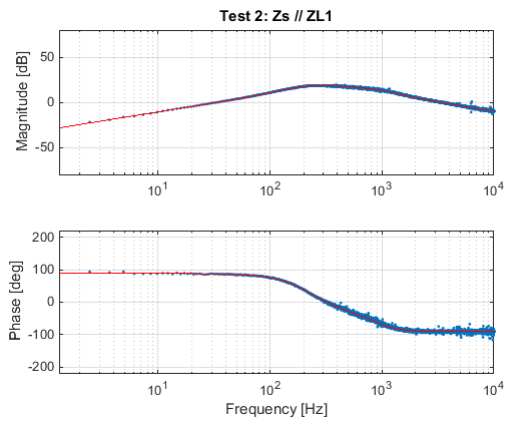


(b)

**Figure 4.11. Test 1: Impedance identification results (dots) compared to the analytic expression (solid line) using (a) single PRBS injection and (b) double PRBS injection**



(a)



(b)

**Figure 4.12. Test 2: Impedance identification results (dots) compared to the analytic expression (solid line) using (a) single PRBS injection and (b) double PRBS injection**

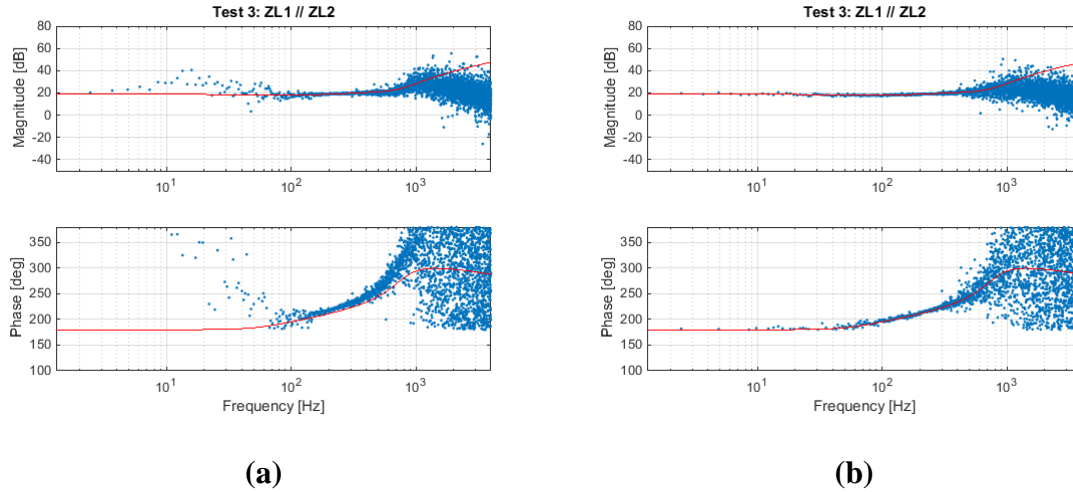


**Figure 4.13. Test 3: Impedance identification results (dots) compared to the analytic expression (solid line) using (a) single PRBS injection and (b) double PRBS injection**

The bus impedance is constructed as in (4.22) and shown in **Figure 4.14** where is compared to the analytic transfer function. A good matching between the estimation and the analytic transfer function is obtained for the frequency range of interest. The identification process gives a finite set of points that represent the non-parametric frequency response. A parametric model of the bus impedance can be obtained by implementing the method of least squares fitting [23].

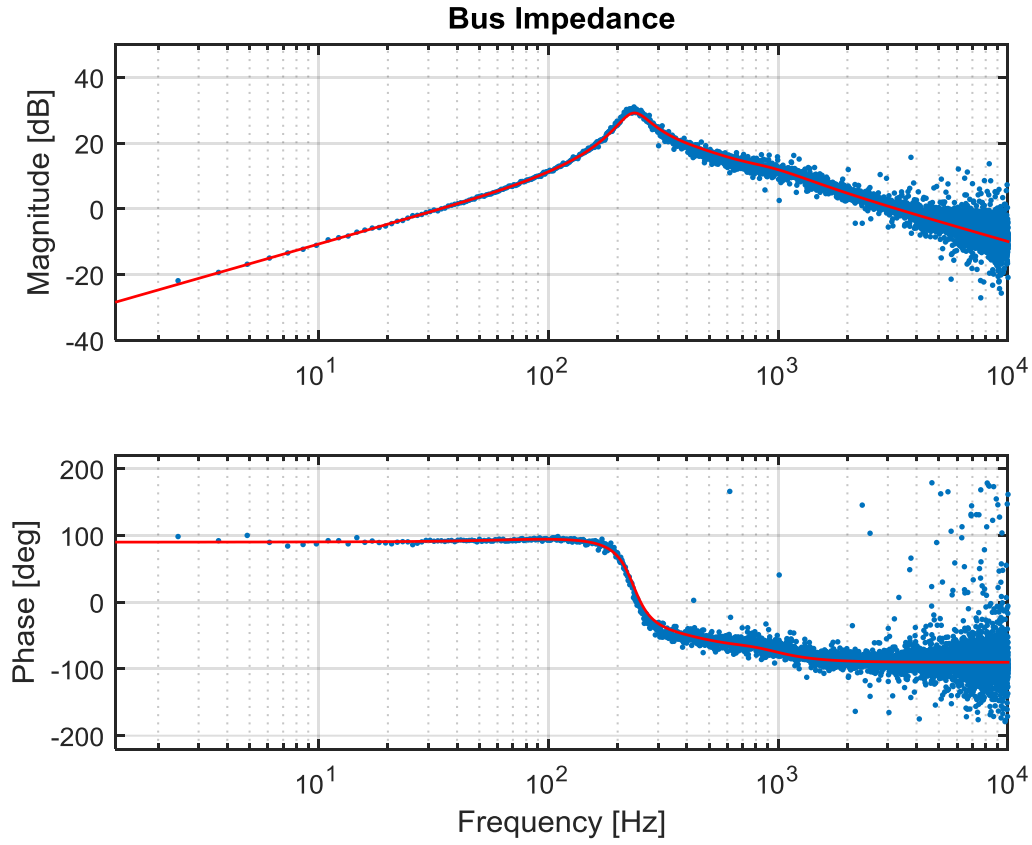


**Figure 4.14. Estimated bus impedance (dots) compared to the analytic transfer function (solid)**

A subset of logarithmically spaced data points, shown in **Figure 4.15**, is utilized in the fitting process in order to enforce equal fitting priority across the frequency range of the measured impedance as seen in the Bode plot with its logarithmic x-axis [14]. This reduces the computational effort in the numerical fitting algorithm.

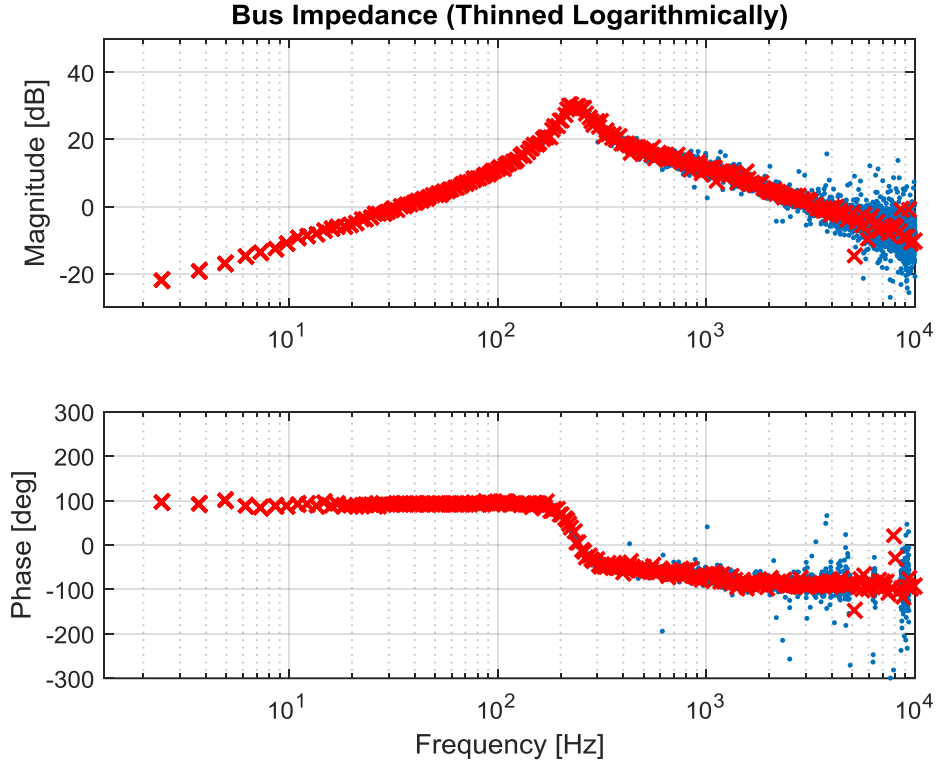


**Figure 4.15.**  $Z_{bus}$  estimated (dots) and logarithmically thinned subset (x mark)

The method of least squares fitting consists in adjusting the coefficients of a candidate transfer function  $Z_{candidate}(s)$  that minimizes the cost function defined by (4.23).

$$J_{WLS} = \frac{1}{2} \sum_k (\varepsilon_k)^2 \quad (4.23)$$

Where  $\varepsilon$  is the error between the candidate transfer function and the measured frequency response.

$$\varepsilon_k = Z_{candidate}(j\omega_k) - Z(j\omega_k) \quad (4.24)$$

The parametric model of the bus impedance in **Figure 4.16** is obtained from the nonparametric complex frequency response. The result is in good agreement with the analytic transfer function, validating the identification process.

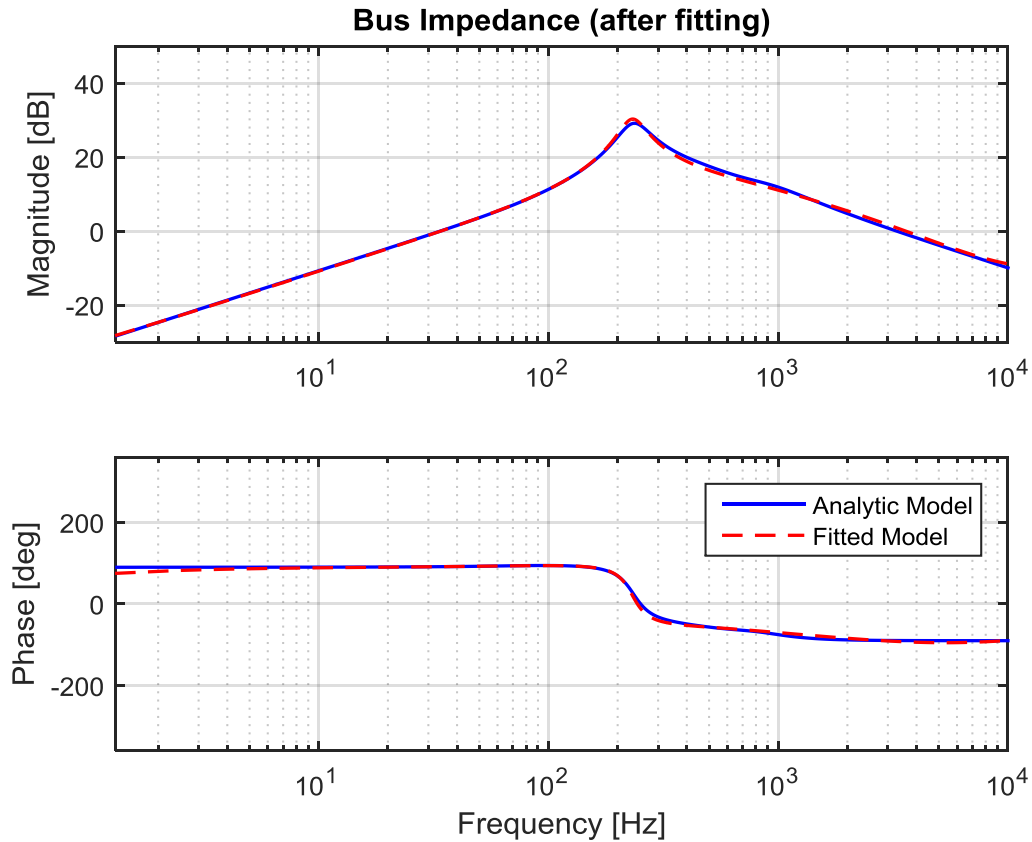


**Figure 4.16. Parametric model of  $Z_{bus}$  (dash) compared to the analytic model (solid).**

#### 4.6. Design of PFF control

Following the approach presented in Section 3.2., the damping impedance that will provide the system with a minimum damping factor of  $\zeta_{min} = 0.5$  is determined from the estimation of the bus impedance.

**Figure 4.17** shows a comparison between the damping impedance obtained from the analytic and parametric models of the bus impedance, giving similar results.

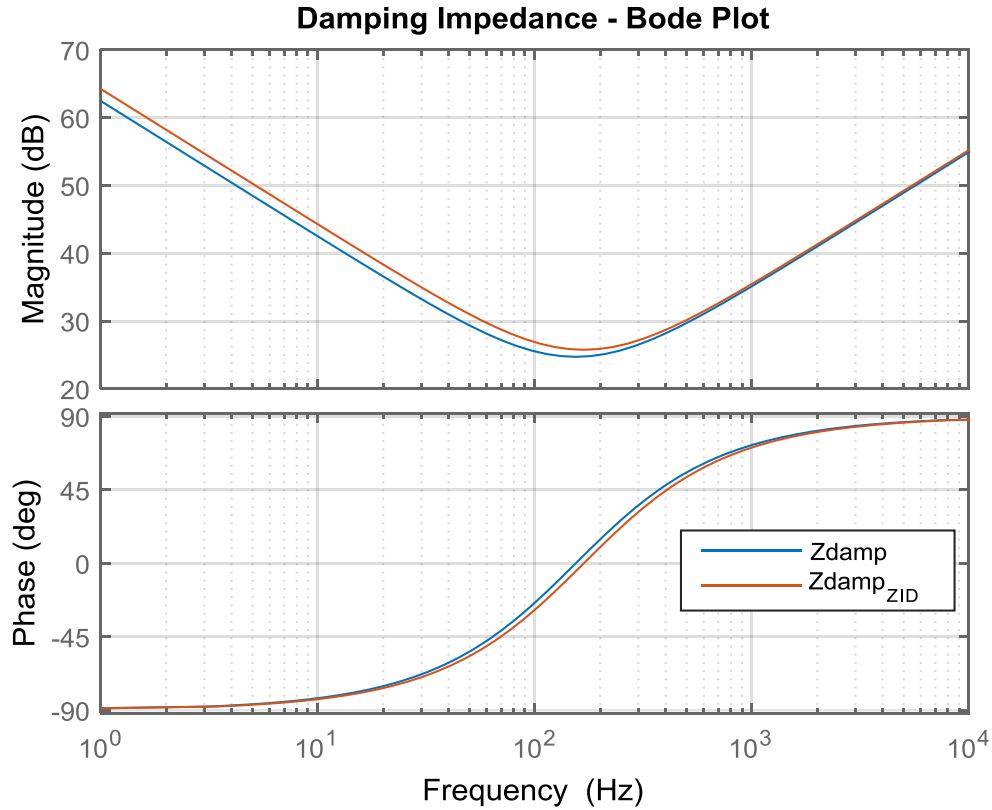


**Figure 4.17. Design of the damping impedance using the analytic model (blue) and the parametric model (red).**

The time domain simulation results are shown in the following figure, where the Positive Feed-Forward control designed from the parametric model is implemented in  $Buck_{LOAD1}$ . The results show well-damped oscillations in correspondence to a step change in the reference voltage of  $Buck_{LOAD2}$ .

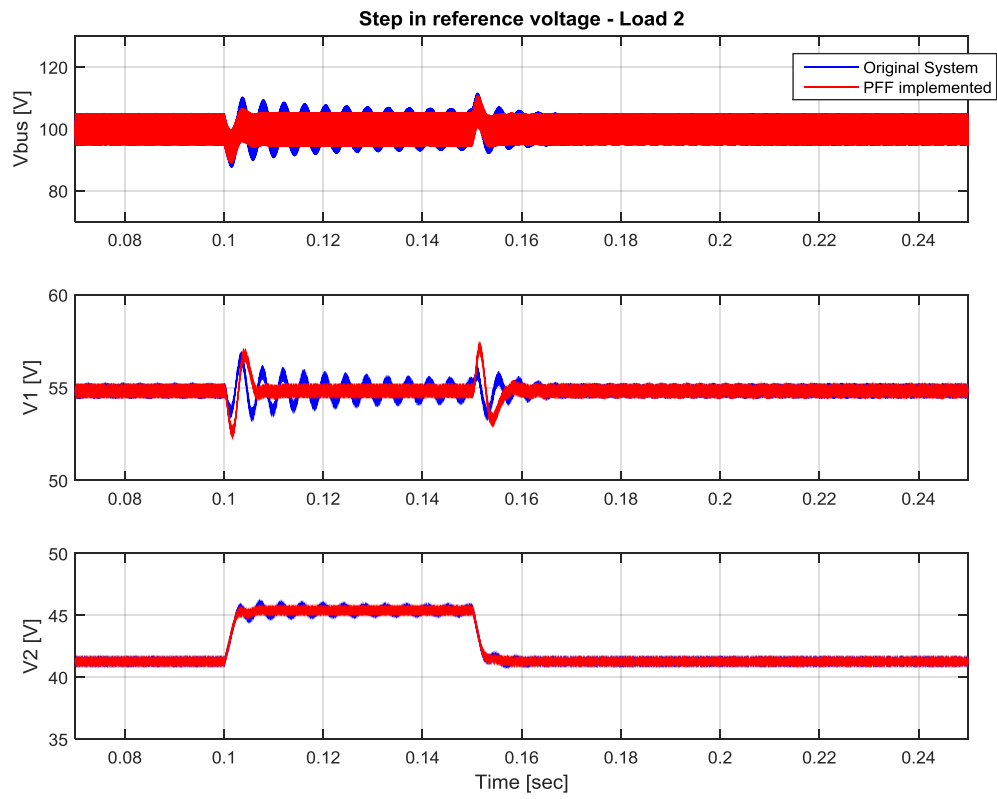


**Figure 4.18.** Time domain simulation results with the implementation of PFF control obtained from the estimation of  $Z_{bus}$ .

## CHAPTER 5

### CONCLUSIONS AND FUTURE WORK

#### 5.1. Conclusions

The main motivation of this work were the issues related to instability in DC Power Distribution Systems caused by the interaction among switching power converters and the necessity for estimating the bus impedance using system identification techniques.

Positive Feed-Forward control is an active approach for improvement of stability margins; it can be designed to place the dominant poles of a DC system bus impedance in a specified location with a desired damping factor. This is important because, as shown in Chapter 2, the bus impedance affects the dynamic response of the system.

Wideband impedance identification is improved by performing double injection of a Pseudo Random Binary Sequence signal as proposed in Chapter 4, allowing a more accurate estimation of the impedance looking out from the converter under test. The significance of the proposed technique is that it can be implemented to estimate the bus impedance by performing local measurements on each converter without the necessity of extra measurement equipment, constituting a low cost solution.

## 5.2. Future Work

### 5.2.1. Online tuning

One of the advantages of the proposed Positive Feed-Forward control design is that it allows the design of a virtual damping impedance to improve stability margins and dynamic characteristics based on measurements obtained from impedance identification techniques.

The impedance identification can be implemented to keep track of the bus impedance variations, which can be used for online tuning of the PFF control based on the most updated estimation of the bus impedance. Particularly this can be performed in the case of load shedding presented in Chapter 2, in which it was shown to be necessary to transfer the PFF control from a disconnected converter to an active converter with a new damping impedance in order to maintain the good dynamic response of the remaining system. A possible adaptive control scheme is shown in **Figure 5.1**.

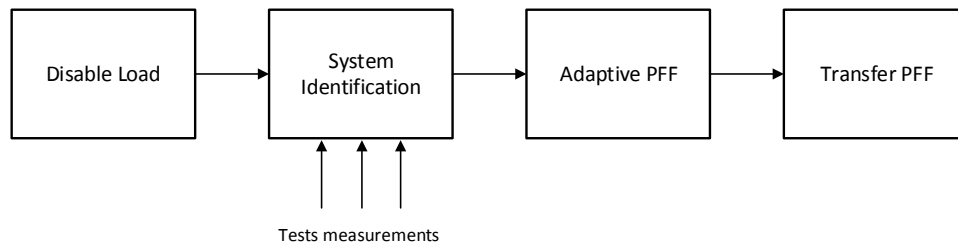


**Figure 5.1. Online tuning scheme.**

### 5.2.2. Experimental Validation

The impedance identification and the implementation of the PFF control was proven to improve the systems dynamics through time domain simulations. It is left as a future task to perform the experimental validation of the proposed method.

## REFERENCES

- [1] IEEE Recommended Practice for 1 kV to 35 kV Medium-Voltage DC Power Systems on Ships, 2010, pp. 1-54.
- [2] M. Cupelli, F. Ponci, G. Sulligoi, A. Vicenzutti, C. Edrington, T. El-Mezyani and A. Monti, "Power flow control and network stability in an all-electric ship," *Proceedings of the IEEE*, vol. 103, no. 12, pp. 2355 - 2380.
- [3] Q. Zhou and D. Yuan, "Prediction on Future DC Power System," *IEEE 6th International Power Electronics and Motion Control Conference*, pp. 1192 - 1195, 2009.
- [4] R. Middlebrook, "Input filter considerations in design and application of switching regulators," *Proc. IEEE Ind. Appl. Soc. Annual Meeting*, pp. 366-382, 1979.
- [5] A. Emadi, A. Khaligh, C. Rivetta and G. Williamson, "Constant power loads and negative impedance instability in automotive systems: definition, modelling, stability, and control of power electronic converters and motor drives," *IEEE Transaction on Vehicular Technology*, vol. 55, no. 4, pp. 1112 - 1125, 2006.
- [6] A. Riccobono and E. Santi, "Comprehensive Review of Stability Criteria for DC Power Distribution Systems," *IEEE Transactions on Industrial Applications*, vol. 50, no. 5, pp. 3525 - 3535, 2014.
- [7] A. Riccobono and E. Santi, "A novel Passivity-Base Stability Criterion (PBSC) for switching converter DC distribution systems," *27th Annual IEEE Applied Power Electronics Conference and Exposition*, pp. 2560 - 2567, 2012.
- [8] A. Riccobono, "Stabilizing controller design for a DC power distribution system using a passivity-based stability criterion," in *Ph.D. dissertation*, University of South Carolina, Columbia, SC, 2013.
- [9] A. Riccobono and E. Santi, "Positive feed-forward control of three-phase voltage source inverter for dc input bus stabilization with experimental validation," *IEEE Transactions on Industry Applications*, vol. 49, no. 1, pp. 168-177, 2013.

- [10] H. Cho and E. Santi, "Modelling and stability analysis in multi-converter systems including positive feedforward control," *34th Annual Conference of IEEE Industrial Electronics*, pp. 839 - 844, 2008.
- [11] H. Cho and E. Santi, "Modelling, control and stability analysis of a converter in multi-converter systems including positive feedforward control," *Ph.D. dissertation, University of South Carolina*, 2009.
- [12] A. Barkley and E. Santi, "Online monitoring of network impedances using digital network analyzer techniques," *Twenty-Fourth Annual IEEE Applied Power Electronics Conference and Exposition*, pp. 440 - 446, 2009.
- [13] D. Martin, E. Santi and A. Barkley, "Wide bandwidth system identification of AC system impedances by applying perturbations to an existing converter," *2011 IEEE Energy Conversion Congress and Exposition*, pp. 2549 - 2556, 2011.
- [14] J. Siegers, S. Arrua and E. Santi, "Stabilizing controller design for multi-bus MVDC distribution systems using a passivity based stability criterion and positive feed-forward control," in *IEEE Energy Conversion Congress and Exposition*, Montreal, 2015.
- [15] A. Barkley, "Online identification, monitoring and control of a DC/DC converter system using digital network analyzer techniques," *PhD Dissertation, University of South Carolina*, 2005.
- [16] R. Erickson and D. Maksimovic, *Fundamentals of Power Electronics*, Springer, 2001.
- [17] J. Maciejowski, *Multivariable Feedback Design*, Addison-Wesley, 1989.
- [18] G. Franklin, J. D. Powell and A. Emami-Naeini, *Feedback Control of Dynamic Systems*, US: Addison-Wesley, 1995.
- [19] J. Proakis and D. Manolakis, "The Discrete Fourier Transform: Its properties and applications," in *Digital Signal Processing*, Pearson, 4th Edition, pp. 464-472.
- [20] B. Miao, R. Zane and D. Maksimovic, "A modified cross-correlation method for system identification of power converters with digital control," *35th Annual IEEE Power Electronics Specialists Conference*, pp. 3728-3733, 2004.
- [21] B. Miao, R. Zane and D. Maksimovic, "System identification of power converters with digital control through cross-correlation methods," *IEEE Transactions on*

*Power Electronics*, vol. 20, no. 5, pp. 1093-1099, 2005.

- [22] A. Barkley and E. Santi, "Improved online identification of a dc-dc converter and its control loop gain using cross-correlation methods," *IEEE Transactions on Power Electronics*, vol. 24, no. 8, pp. 2021-2031, 2009.
- [23] D. Martin, "Applications of power electronics converter based wideband system identification in grid tied AC power systems," in *Ph.D. dissertation*, University of South Carolina. Columbia, SC, 2012.
- [24] K. Astrom and B. Wittenmark, *Computer-Controlled Systems*, Dover, 2014.
- [25] X. Zhang and X. Ruan, "Adaptive active capacitor converter for improving stability of cascaded dc power supply system," *IEEE Transactions on Power Electronics*, vol. 28, no. 4, pp. 1807 - 1816, April 2013.